Global Correlations of Ocean Ridge Basalt Chemistry with Axial Depth: a New Perspective

YAOLING NIU[1]* AND MICHAEL J. O'HARA[2]

[1]DEPARTMENT OF EARTH SCIENCES, DURHAM UNIVERSITY, DURHAM DH1 3LE, UK
[2]INSTITUTE OF GEOGRAPHY AND EARTH STUDIES, ABERYSTWYTH UNIVERSITY, ABERYSTWYTH SY23 3DB, UK

The petrological parameters Na_8 and Fe_8, which are Na_2O and FeO contents in mid-ocean ridge basalt (MORB) melts corrected for fractionation effects to $MgO = 8 wt\%$, have been widely used as indicators of the extent and pressure of mantle melting beneath ocean ridges. We find that these parameters are unreliable. Fe_8 is used to compute the mantle solidus depth (P_o) and temperature (T_o), and it is the values and range of Fe_8 that have led to the notion that mantle potential temperature variation of $\Delta T_P = 250 K$ is required to explain the global ocean ridge systematics. This interpreted $\Delta T_P = 250 K$ range applies to ocean ridges away from 'hotspots'. We find no convincing evidence that calculated values for P_o, T_o, and ΔT_P using Fe_8 have any significance. We correct for fractionation effect to $Mg^\# = 0.72$, which reveals mostly signals of mantle processes because melts with $Mg^\# = 0.72$ are in equilibrium with mantle olivine of $Fo_{89.6}$ (vs evolved olivine of $Fo_{88.1-79.6}$ in equilibrium with melts of Fe_8). To reveal first-order MORB chemical systematics as a function of ridge axial depth, we average out possible effects of spreading rate variation, local-scale mantle source heterogeneity, melting region geometry variation, and dynamic topography on regional and segment scales by using actual sample depths, regardless of geographical location, within each of 22 ridge depth intervals of 250 m on a global scale. These depth-interval averages give $Fe_{72} = 7.5–8.5$, which would give $\Delta T_P = 41 K$ (vs ~250 K based on Fe_8) beneath global ocean ridges. The lack of $Fe_{72}–Si_{72}$ and Si_{72}–ridge depth correlations provides no evidence that MORB melts preserve pressure signatures as a function of ridge axial depth. We thus find no convincing evidence for $\Delta T_P > 50 K$ beneath global ocean ridges. The averages have also revealed significant correlations of MORB chemistry (e.g. Ti_{72}, Al_{72}, Fe_{72}, Mg_{72}, Ca_{72}, Na_{72} and Ca_{72}/Al_{72}) with ridge axial depth. The chemistry–depth correlation points to an intrinsic link between the two. That is, the ~5 km global ridge axial relief and MORB chemistry both result from a common cause: subsolidus mantle compositional variation (vs ΔT_P), which determines the mineralogy, lithology and density variations that (1) isostatically compensate the ~5 km ocean ridge relief and (2) determine the first-order MORB compositional variation on a global scale. A progressively more enriched (or less depleted) fertile peridotite source (i.e. high Al_2O_3 and Na_2O, and low CaO/Al_2O_3) beneath deep ridges ensures a greater amount of modal garnet (high Al_2O_3) and higher jadeite/diopside ratios in clinopyroxene (high Na_2O and Al_2O_3, and lower CaO), making a denser mantle, and thus deeper ridges. The dense fertile mantle beneath deep ridges retards the rate and restricts the amplitude of the upwelling, reduces the rate and extent of decompression melting, gives way to conductive cooling to a deep level, forces melting to stop at such a deep level, leads to a short melting column, and thus produces less melt and probably a thin magmatic crust relative to the less dense (more refractory) fertile mantle beneath shallow ridges. Compositions of primitive MORB melts result from the combination of two different, but genetically related processes: (1) mantle source inheritance and (2) melting process enhancement. The subsolidus mantle compositional variation needed to explain MORB chemistry and ridge axial depth variation requires a deep isostatic compensation depth, probably in the transition zone. Therefore, although ocean ridges are of shallow origin, their working is largely controlled by deep processes as well as the effect of plate spreading rate variation at shallow levels.

INTRODUCTION

The global mid-ocean ridge system is the dynamic manifestation of mantle convection that governs plate

*Corresponding author. Telephone: +44-19-1334-2311. Fax: +44-19-1334-2301. E-mail: Yaoling.Niu@durham.ac.uk

tectonics. Our current understanding of ocean ridge magmatism, which creates the ocean crust, results from multidisciplinary efforts. Seafloor geological and geophysical observations have laid the foundation. Surface-ship dredging, submersibles, and deep-sea drilling have collected the magmatic products to infer magmatic processes. Theoretical considerations have established that ocean ridges are mostly passive features in the sense that the mantle beneath the ridge rises adiabatically and melts by decompression in response to plate separation. Experimental petrology has been particularly important in facilitating interpretations of mid-ocean ridge basalts (MORB) in terms of physical processes of mantle melting and magma evolution. Dave Green has been one of the pioneers (Green & Ringwood, 1963, 1964, 1967, 1970; O'Hara & Yoder, 1963, 1967; O'Hara, 1965, 1967, 1968a, 1968b, 1970; Green, 1971, 1973; Wyllie, 1973; Green et al., 1979; Presnall et al., 1979; Jaques & Green, 1980; Stolper, 1980; Falloon & Green, 1987, 1988; Green & Falloon, 1998, 2005) in using peridotite melting experiments to study MORB petrogenesis.

The paper by Jaques & Green (1980) in particular marked a turning point for MORB petrogenesis research. It demonstrated for the first time how the bulk compositions of partial melts of mantle peridotite vary systematically with melting conditions and mantle composition, and thus laid the groundwork for the establishment of detailed petrogenetic grids and empirical models aimed at a quantitative understanding of ocean ridge melting and MORB genesis (e.g. Klein & Langmuir, 1987; McKenzie & Bickle, 1988; Niu & Batiza, 1991a; Kinzler & Grove, 1992; Langmuir et al., 1992; Kinzler, 1997; Niu, 1997). Figure 1, which summarizes the model results of Niu (1997), illustrates the concept of Jaques & Green (1980).

The paper by Klein & Langmuir (1987) is a milestone contribution on MORB genesis. Following the idea of Dick & Fisher (1984) and Dick et al. (1984), Klein & Langmuir (1987) showed that location-averaged MORB chemistry correlates with ridge axial depth on a global scale. For example, Fe_8 (i.e. FeO corrected for the effect of crystal fractionation to MgO = 8 wt%) increases whereas Na_8 decreases as the ridge shallows (Fig. 2a and b). They interpreted such correlations as resulting from varying pressures and degrees of partial melting of a compositionally uniform mantle (Fig. 2c) caused by temperature variation in the subsolidus mantle of up to 250 K from beneath cold deep ridges to hot shallow ridges with a compensation depth of 150–200 km. In a more comprehensive treatment, Langmuir et al. (1992) re-examined the same problem further and confirmed the basic conclusions of Klein & Langmuir (1987).

These interpretations have been widely accepted as the way the mantle actually works despite numerous arguments for alternative working hypotheses
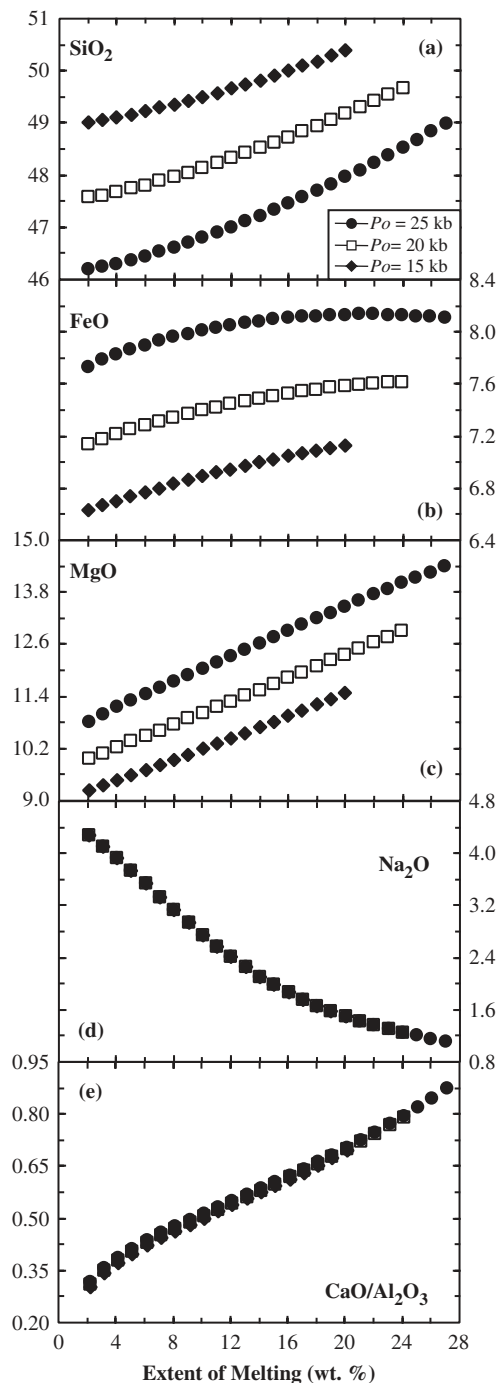

Fig. 1. Model compositions of mantle melts produced by decompression melting to illustrate that compositions of primary mantle melts vary as a function of initial melting depth (e.g. P_o = 25, 20 and 15 kbar) and the extent of melting. The decompression melting models use the parameterization and fertile source composition given by Niu (1997). The decompression melting is arbitrarily stopped at ∼8 kbar for all three melting paths. Such parameterization is possible (e.g. Niu & Batiza, 1991a) because of the critical peridotite melting experiments by Jaques & Green (1980) and similar sets of experimental data available subsequently (e.g. Falloon & Green, 1987, 1988; Falloon et al., 1988; Hirose & Kushiro, 1993; Baker & Stolper, 1994).
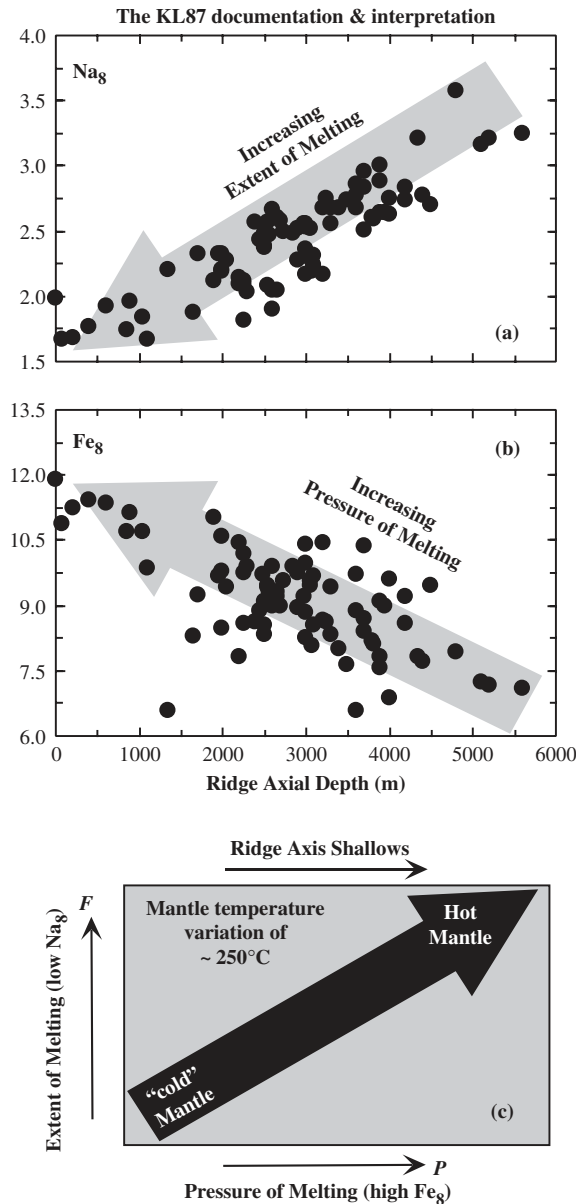
Fig. 2. (a) and (b) Summary plots of location averaged global MORB compositions as a function of ocean ridge axial depth documented by Klein & Langmuir (1987) (KL87), where Na$_8$ and Fe$_8$ are the corresponding Na$_2$O and FeO (wt%) in MORB melts corrected for fractionation effects to MgO = 8 wt%. (c) Schematic illustration of their interpretation: a hotter mantle melts deeper (high Fe$_8$) and melts more (low Na$_8$) than a cooler mantle. The interpretation is deduced from the peridotite melting experiments of Jaques & Green (1980) as modeled by Niu (1997) in Fig. 1.

(Brodholt & Batiza, 1989; Natland, 1989; Albarède, 1992; Niu & Batiza, 1993, 1994; Shen & Forsyth, 1995; Niu, 1997, 2004; Niu & Hékinian, 1997a, 1997b; Castillo *et al.*, 1998, 2000; Niu *et al.*, 2001, 2002; Presnall *et al.*, 2002; Presnall & Gudfinnsson, this issue).
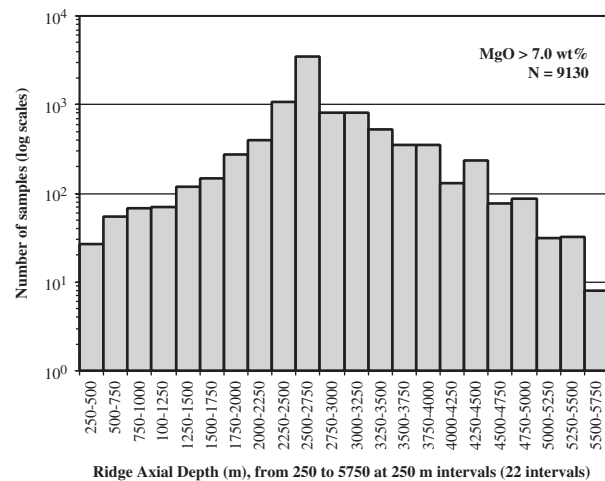
Fig. 3. Histogram showing the distribution of the global MORB samples considered in this study as a function of ridge axial depth. All MORB glass data are from the 'Petrological Database of the Ocean Floor (PETDB)' (www.petdb.org). To minimize the need for fractionation correction, we choose to use samples with MgO >7 wt%, which leaves 9130 samples to work with.

In this paper we re-examine the Klein & Langmuir (1987) and Langmuir *et al.* (1992) interpretations, in particular the argument for 250 K mantle temperature variation and the suggestion for a compensation depth of 150–200 km required to explain global ridge axial depth variations. We offer an alternative approach for fractionation correction. We conclude that mantle temperature variation is likely to be inadequate and that a significant contribution from mantle compositional variation is required to explain global axial depth and MORB compositional variations and correlations on a global scale.

THE GLOBAL MORB DATASET AND NEW PERSPECTIVES

About 13 900 glass analyses are available in the global MORB database (PetDB, http://beta.www.petdb.org/). In our analyses, we have excluded samples (1) with SiO$_2$ >53 wt% (up to 71 wt%, basaltic andesite to rhyolite), (2) without water depth information, (3) from depths <400 m to minimize any 'hotspot' effect, and (4) with MgO <7 wt% to avoid unnecessary errors associated with fractionation correction for the more evolved samples because of the non-linear liquid lines of descent (LLDs) for most oxides (see Electronic Appendix A, available for downloading at http://www.petrology.oxfordjournals.org/). This leaves 9130 samples on a global scale to work with.

Figure 3 shows sample distribution with ridge axial depth. A logarithmic scale is used to magnify the details at both deep and shallow ridge depths. This log-normal

sample distribution largely reflects the ridge axial depth variation on a global scale. Much of the global mid-ocean ridge lies between 2000 and 3000 m water depth in geographical regions readily accessible for sampling.

As expected, compositions of samples vary significantly along ridge segments and with respect to physical observables such as spreading rate (Niu & Batiza, 1993; Niu & Hékinian, 1997a, 1997b) or ridge axial depth on all scales (Brodholt & Batiza, 1989; Niu & Batiza, 1993, 1994; Niu et al., 2001). In this case, averaging is often used to 'average out' outliers or reduce the scatter in pursuit of first-order systematics (e.g. Klein & Langmuir, 1987; Langmuir et al., 1992; Niu & Hékinian, 1997a; Rubin & Sinton, 2007). The way to average is not arbitrary, but follows some basic principles. As long as the analytical data are of good quality, there is no reason to exclude arbitrarily any 'outliers' because each analysis, whatever its composition may be, results from compound mantle processes. Assuming that the shallow-level fractional crystallization effect can be effectively removed (see below), the data still possess the signatures of fertile mantle compositional (lithological and mineralogical) variation on all scales, spreading-rate dependent variation, mean pressures of melting, and mantle temperature variation (Niu et al., 2001). The way to effectively deconvolve all these probable effects is to average the data with respect to a particular variable. For example, to examine the effect of spreading rate variation on MORB chemistry, we must average the MORB data with respect to spreading rate within chosen spreading rate windows (Niu & Hékinian, 1997a; Rubin & Sinton, 2007). To examine if MORB chemistry varies with ridge axial depth, we must average the MORB data with respect to ridge axial depth within chosen depth intervals. This is mathematically the same as seeking the partial derivatives of a quantity with respect to a particular variable, with all other variables held constant.

There are two factors to consider when averaging MORB data with respect to ridge axial depth:

(1) The global ridge axial depth varies from near sea level at the Reykjanes Ridge immediately south of Iceland to as deep as 6000 m in portions of the Cayman Rise. What would be the ideal depth interval to average? We choose a 250 m depth interval because this value approximates the ridge depth variation over ~500 km regional-scale lengths and because we will have >20 averaged data points to work with. This number of data points is large enough to be statistically significant without compromising first-order systematics, but is small enough to smooth out secondary effects while making the first-order global systematics prominent.

(2) Ridge axial depth can vary significantly on ridge segment scales, in particular along slow-spreading ridges such as the Mid-Atlantic Ridge (MAR). For example, within the ~90 km long MAR ridge segment at ~26°S (Niu & Batiza, 1994), the axis is ~2500 m deep at the segment center, but deepens to ~4000 m towards segment offsets.

How to do the averaging?

Klein & Langmuir (1987) chose to smooth the variation in ridge depth by using a derived single depth value for all samples from a particular ridge segment. Such smoothing of ridge depth is arbitrary, and such 'pre-treatment' of a physical observable potentially loses information. In contrast, we use the actual depths at which basalt samples were erupted in this study. Table 1 gives the averages for samples within each of the 22 depth intervals (Fig. 3). To minimize the Iceland 'hotspot' effect, we exclude samples in the 0–250 m depth interval. As there are no samples in the 250–400 m depth range with MgO >7 wt%, the 250–500 m depth interval actually includes only samples from the ridge axis at depths >400 m. We thus have 22 depth intervals of 250 m or 22 averaged data points to work with (see Fig. 3).

Chemistry–depth correlations: averages of fractionation-uncorrected raw data

Table 1 gives depth-interval averages of fractionation-uncorrected major (SiO_2, TiO_2, Al_2O_3, FeO_t, MgO, CaO and Na_2O) and minor (MnO, K_2O and P_2O_5) element oxides. Figure 4 shows that TiO_2, Al_2O_3, Na_2O and $Mg^{\#}$ increase whereas FeO, CaO and CaO/Al_2O_3 decrease with increasing ridge axial depth. The MgO–depth correlation is less significant partly because of the use of samples with MgO >7 wt% only. All these correlations are statistically significant at the >95% confidence level. SiO_2 and the minor oxides MnO and P_2O_5 do not show systematic variation vs ridge axial depth. However, Fig. 5a shows, despite a higher value 'outlier' in the depth interval 2000–2250 m, that K_2O does show a statistically significant decrease towards shallower ridges.

Except for the inverse CaO/Al_2O_3–depth correlation shown by Klein & Langmuir (1987) and Brodholt & Batiza (1989) and the associations of high-Na_2O MORB with deep ridges and low-Na_2O MORB with shallow ridges identified by Bryan & Dick (1982), Dick & Fisher (1984), Dick et al. (1984) and Brodholt & Batiza (1989), Table 1 and Figures 4 and 5a represent the first demonstration that most major and minor element oxides (except SiO_2, MnO and P_2O_5) in global MORB melts correlate with ridge axial depth, and such correlations are more prominent when depth-interval averages are plotted.

The decreasing $Mg^{\#}$ in MORB melts from deep ridges ($Mg^{\#}$ ~0·68) to shallow ridges ($Mg^{\#}$ ~0·55) (Fig. 4) is consistent with, and best explained by, advanced degrees of fractional crystallization towards shallow ridges (lowering $Mg^{\#}$). However, the systematics of other oxides
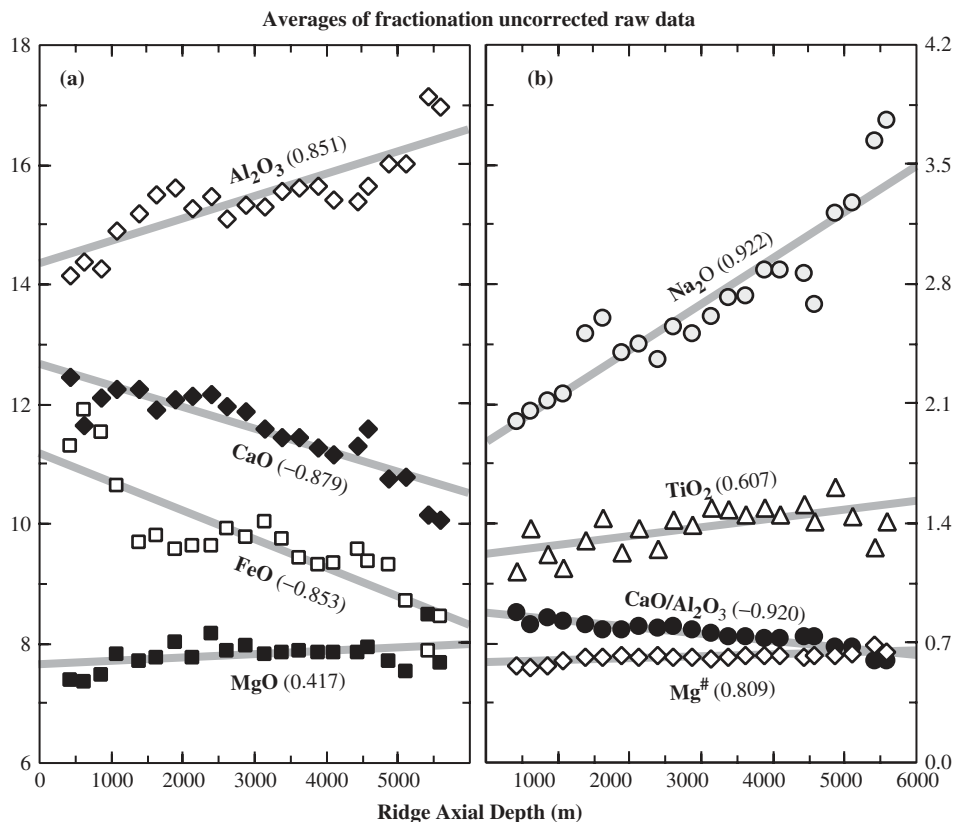
Table 1: Ridge depth interval (250 m) averages of global MORB major element data: averages with standard deviations of raw data

Depth interval (m)	n	Depth (m)	1σ	SiO_2	1σ	TiO_2	1σ	Al_2O_3	1σ	FeO_t	1σ	MnO	1σ	MgO	1σ
250–500	27	425	23	50·538	0·335	1·117	0·173	14·150	0·299	11·298	0·721	0·197	0·031	7·382	0·353
500–750	55	633	51	50·593	0·568	1·372	0·189	14·385	0·441	11·899	0·886	0·130	0·059	7·360	0·505
750–1000	68	856	78	50·940	0·650	1·221	0·135	14·263	0·464	11·524	1·089	0·169	0·028	7·476	0·637
1000–1250	71	1084	78	50·389	1·039	1·142	0·218	14·886	0·935	10·647	1·448	0·163	0·027	7·820	0·672
1250–1500	120	1397	83	50·491	0·861	1·304	0·367	15·191	0·766	9·683	0·993	0·175	0·063	7·684	0·688
1500–1750	149	1635	85	50·241	1·110	1·434	0·281	15·498	0·970	9·789	1·016	0·178	0·045	7·756	0·643
1750–2000	278	1904	74	50·220	1·300	1·233	0·294	15·611	1·086	9·582	0·828	0·169	0·028	8·024	0·676
2000–2250	400	2148	79	50·519	0·743	1·374	0·257	15·272	0·750	9·624	1·130	0·174	0·035	7·750	0·563
2250–2500	1060	2402	71	50·342	0·851	1·253	0·307	15·481	0·829	9·619	0·790	0·176	0·036	8·146	0·797
2500–2750	3434	2619	70	50·446	0·643	1·425	0·316	15·105	0·689	9·904	0·818	0·184	0·043	7·876	0·629
2750–3000	817	2873	68	50·470	0·698	1·393	0·320	15·337	0·764	9·756	0·875	0·177	0·033	7·965	0·647
3000–3250	820	3132	74	50·394	0·761	1·491	0·316	15·307	0·735	10·036	0·980	0·183	0·029	7·811	0·573
3250–3500	531	3376	76	50·381	0·690	1·483	0·237	15·566	0·752	9·743	0·788	0·176	0·033	7·849	0·510
3500–3750	346	3625	81	50·659	0·796	1·447	0·264	15·602	0·666	9·438	0·762	0·170	0·028	7·879	0·624
3750–4000	348	3886	71	50·744	0·771	1·490	0·232	15·639	0·703	9·308	0·771	0·170	0·028	7·834	0·604
4000–4250	132	4093	57	50·814	0·669	1·448	0·171	15·398	0·591	9·345	0·728	0·179	0·031	7·848	0·480
4250–4500	238	4431	57	50·537	0·665	1·515	0·196	15·390	0·444	9·576	0·661	0·173	0·040	7·837	0·478
4500–4750	77	4585	44	50·765	0·891	1·412	0·240	15·649	0·691	9·359	0·777	0·174	0·031	7·942	0·643
4750–5000	88	4863	78	50·528	0·740	1·607	0·289	16·024	0·771	9·319	0·788	0·176	0·024	7·696	0·498
5000–5250	31	5113	57	50·885	0·487	1·438	0·249	16·017	1·126	8·710	0·952	0·166	0·025	7·515	0·403
5250–5500	32	5428	19	50·777	0·344	1·257	0·152	17·135	0·375	7·871	0·300	0·174	0·017	8·462	0·397
5500–5750	8	5600	0	50·420	0·209	1·410	0·019	16·978	0·050	8·449	0·072	0·155	0·008	7·681	0·082

Depth interval (m)	CaO	1σ	Na_2O	1σ	K_2O	1σ	P_2O_5	1σ	Sum	1σ	$Mg^{\#}$	1σ	CaO/Al_2O_3	1σ	K_2O/TiO_2	1σ
250–500	12·442	0·345	1·996	0·056	0·104	0·055	0·100	0·035	99·27	0·48	0·564	0·027	0·879	0·020	0·134	0·087
500–750	11·646	0·408	2·053	0·106	0·132	0·048	0·143	0·029	99·59	0·54	0·550	0·034	0·810	0·026	0·131	0·043
750–1000	12·098	0·419	2·110	0·167	0·097	0·147	0·114	0·038	99·86	0·63	0·562	0·041	0·849	0·036	0·096	0·124
1000–1250	12·247	0·670	2·152	0·344	0·108	0·158	0·104	0·046	99·50	0·63	0·593	0·048	0·825	0·059	0·110	0·142
1250–1500	12·256	0·629	2·504	0·525	0·149	0·116	0·146	0·046	99·43	0·68	0·611	0·038	0·809	0·054	0·144	0·109
1500–1750	11·912	0·534	2·599	0·326	0·170	0·151	0·155	0·046	99·57	0·65	0·611	0·040	0·772	0·059	0·161	0·130
1750–2000	12·058	0·603	2·398	0·295	0·179	0·149	0·131	0·064	99·49	0·49	0·623	0·033	0·776	0·066	0·182	0·142
2000–2250	12·117	0·657	2·450	0·324	0·253	0·229	0·160	0·060	99·57	0·61	0·615	0·037	0·795	0·055	0·245	0·217
2250–2500	12·160	0·746	2·352	0·355	0·135	0·131	0·128	0·050	99·65	0·53	0·625	0·037	0·787	0·059	0·144	0·128
2500–2750	11·966	0·495	2·546	0·310	0·126	0·072	0·142	0·050	99·62	0·59	0·611	0·035	0·793	0·038	0·122	0·065
2750–3000	11·864	0·600	2·508	0·344	0·137	0·113	0·152	0·076	99·65	0·54	0·617	0·036	0·775	0·050	0·134	0·099
3000–3250	11·581	0·609	2·612	0·323	0·139	0·092	0·146	0·043	99·59	0·57	0·606	0·036	0·758	0·052	0·129	0·079
3250–3500	11·449	0·567	2·722	0·273	0·130	0·086	0·150	0·039	99·51	0·66	0·615	0·030	0·737	0·048	0·119	0·074
3500–3750	11·432	0·428	2·729	0·288	0·157	0·117	0·151	0·038	99·54	0·53	0·623	0·032	0·734	0·035	0·151	0·117
3750–4000	11·270	0·514	2·879	0·341	0·159	0·152	0·156	0·044	99·53	0·55	0·625	0·030	0·722	0·050	0·147	0·137
4000–4250	11·154	0·566	2·881	0·281	0·121	0·073	0·142	0·030	99·22	0·75	0·625	0·024	0·725	0·042	0·117	0·071
4250–4500	11·299	0·538	2·856	0·254	0·132	0·055	0·155	0·043	99·38	0·65	0·618	0·026	0·735	0·042	0·120	0·045
4500–4750	11·574	0·668	2·680	0·310	0·143	0·084	0·150	0·031	99·71	0·56	0·626	0·035	0·740	0·038	0·137	0·070
4750–5000	10·749	0·683	3·209	0·411	0·159	0·068	0·163	0·040	99·54	0·66	0·621	0·027	0·672	0·055	0·138	0·058
5000–5250	10·763	0·783	3·277	0·632	0·179	0·078	0·136	0·055	99·00	0·61	0·632	0·025	0·677	0·089	0·175	0·080
5250–5500	10·146	0·173	3·641	0·110	0·210	0·019	0·156	0·018	99·65	0·36	0·680	0·019	0·592	0·017	0·234	0·033
5500–5750	10·044	0·069	3·754	0·060	0·178	0·010	0·104	0·021	99·17	0·19	0·643	0·002	0·592	0·004	0·174	0·010

Fig. 4. Plots of ridge-depth interval averages (Fig. 3; data from Table 1) of fractionation-uncorrected MORB major element oxide data [Al_2O_3, FeO, MgO and CaO in (a); TiO_2, Na_2O, CaO/Al_2O_3 and $Mg^{\#}$ in (b)], showing statistically significant (at a >99% confidence level for all but MgO, which is at >95% confidence level) correlations with ridge axial depth on a global scale.

(except Al_2O_3, MgO and, to a lesser extent, FeO in a qualitative sense) with ridge axial depth cannot be readily explained by the same process acting on a similar parental magma. Hence, part of the fractionation-uncorrected MORB compositional variation as a function of ridge axial depth must reflect parental magma compositional variation with ridge axial depth. We will address in subsequent sections why MORB parental melt composition varies with ridge axial depth and why parental melts delivered to shallow ridges crystallize (evolve) more than those delivered to deep ridges.

CORRECTION FOR FRACTIONATION EFFECTS

It is well established that MORB melts are not primary magmas, but are variably evolved derivatives, primarily through fractional crystallization as a result of cooling at shallow levels (e.g. O'Hara, 1968a; Walker et al., 1979; Stolper, 1980; Langmuir, 1989; Sinton & Detrick, 1992; O'Hara & Herzberg, 2002). Therefore, to see the mantle signals that MORB melts might preserve, it is

necessary to correct for the effect of crustal-level fractional crystallization.

The Klein & Langmuir (1987) method and interpretations

It is not possible to correct unambiguously the effect of fractional crystallization back to the status of primary magmas because the exact fractionation processes are unknown. Klein & Langmuir (1987, p. 8090) arbitrarily chose to correct to MgO = 8 wt%. The correction is made on Na_2O–MgO and FeO–MgO variation diagrams by back-tracking along LLDs for samples with MgO <8 wt% and forward for samples with MgO >8 wt% to MgO = 8 wt%. Klein & Langmuir (1987) excluded samples with MgO <5 wt% to avoid possible correction errors. MORB melts from different ridges can have different LLDs, and different LLDs can exist in a given ridge segment. However, the LLDs often define parallel or sub-parallel trends on MgO variation diagrams. Hence, applying a single set of LLD slopes for Na_2O–MgO and FeO–MgO to the global database is acceptable [see Klein & Langmuir (1987, fig. 2) and also Langmuir et al. (1992)]. Na_8 and Fe_8 (Fig. 2) are such fractionation-corrected values
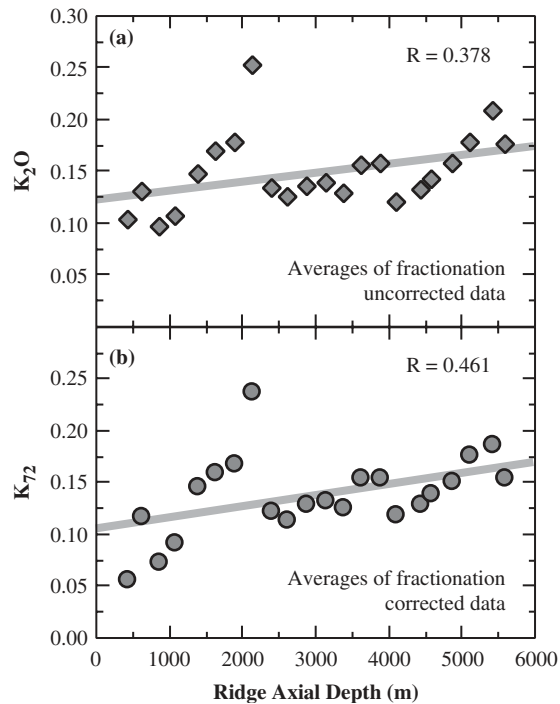
Fig. 5. (a) Averages of fractionation-uncorrected K_2O wt% vs ridge axial depth. There is a high value 'outlier' in the depth interval 2000–2250 m. The overall declining trend towards shallower ridges is statistically significant at a >90% confidence level. (b) Averages of fractionation-corrected K_{72} vs ridge axial depth; the correlation is statistically significant at a >95% confidence level.

for Na_2O and FeO at $MgO = 8.0$ wt% in MORB melts by Klein & Langmuir (1987) and Langmuir *et al.* (1992). Na_8 and Fe_8 are now well-known petrological parameters widely used to indicate the extents and pressures of mantle melting required to generate MORB, and basalts from ocean islands and other tectonic settings, including continental flood basalts.

Figure 1 shows that, in primary melts, Na_2O decreases with increasing degree of melting and FeO is higher in higher pressure melts (Jaques & Green, 1980). Consequently, Klein & Langmuir (1987) interpreted the correlations of MORB Na_8 and Fe_8 with ridge axial depth (Fig. 2) as resulting from varying extents and pressures of melting caused by temperature variation of up to 250 K in the subsolidus mantle from beneath cold deep ridges to hot shallow ridges. It should be noted that Klein & Langmuir (1987) did not use mantle potential temperature, T_B defined by McKenzie & Bickle (1988), but their 'subsolidus mantle temperature variation' can be conceptually referred to as temperature variation at the mantle solidus ($T_{Solidus}$), so that both can be compared by the linear relationship $T_P = T_{Solidus} − P_{Solidus}(kbar) \times 1.8°C/kbar$, where $1.8°C/kbar$ is the assumed adiabat (McKenzie & Bickle, 1988). $T_{Solidus}$ (or T_o) and $P_{Solidus}$ (or P_o) are explicitly the temperature and pressure at which the ascending mantle intersects the solidus.
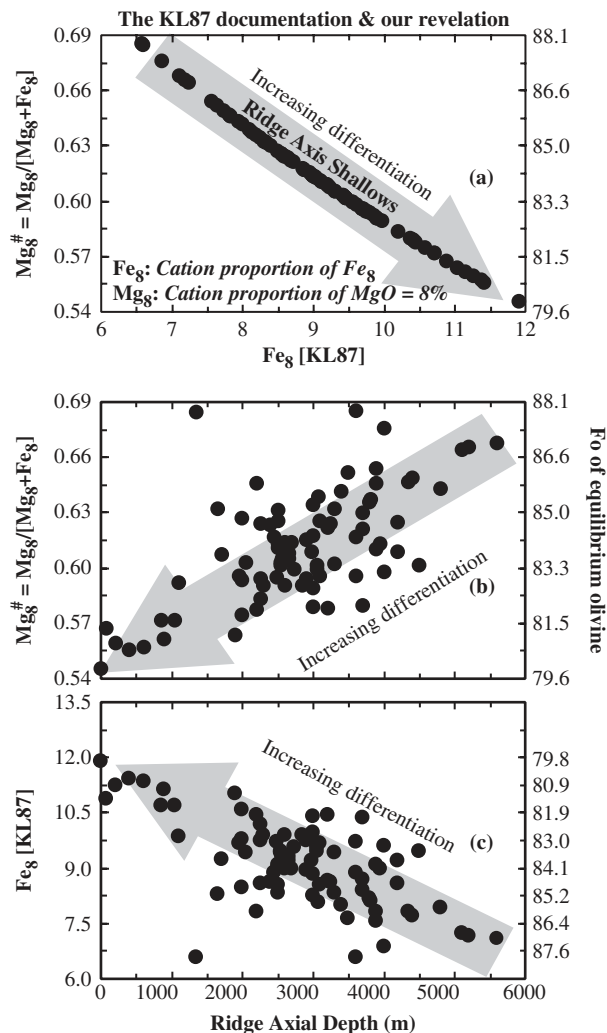
The problem of the Fe_8 correction of Klein & Langmuir (1987)

The hidden problem in the concept of fractionation correction of FeO to Fe_8 is revealed by calculating $Mg^{\#} = Mg_8/(Mg_8 + Fe_8)$, where Mg_8 is the cation proportion of Mg at $MgO = 8$ wt%, and Fe_8 is the cation proportion of Fe at at $MgO = 8$ wt%. Figure 6a demonstrates that Klein & Langmuir's (1987) Fe_8 values for the global MORB dataset correlate inversely with $Mg^{\#}$. This correlation suggests that the Klein & Langmuir (1987) fractionation-corrected data still largely reflect varying degrees of fractional crystallization from less evolved melts (e.g. $Mg^{\#} \sim 0.68$) to highly evolved melts (e.g. $Mg^{\#} \sim 0.55$), which does not relate in any straightforward way to depth of mantle melting and mantle potential temperature variation.

Klein & Langmuir's (1987) inverse Fe_8–depth correlation in Fig. 2b (reproduced in Fig. 6c for comparison) is conceptually identical to the positive $Mg^{\#}$–depth correlation (Fig. 6b). That is, $Mg^{\#}$ decreases from ~ 0.68 at deep ridges to ~ 0.55 at shallow ridges. These melts can only be in equilibrium with highly evolved Fe-rich olivine of $Fo_{79.6–88.1}$ (Fig. 6a and b), not with mantle olivine of $Fo > 89.5$ (e.g. Roeder & Emslie, 1970). Therefore, by using Fe_8 (total range 7 to ~ 11) one examines the progressively more evolved melt, mostly at the crustal level, from deep ridges to shallow ridges, not the pressures of mantle melting.

Another hidden problem in the concept of the Fe_8 correction is that using a constant MgO value (8 wt%) results in the loss of the intrinsically positive FeO–MgO correlation obvious in model primary melts (Fig. 1) (Niu & Batiza, 1991*a*; Niu, 1997; Herzberg & O'Hara, 1998, 2002) and melts of peridotite melting experiments (e.g. Jaques & Green, 1980; Falloon & Green, 1987, 1988; Falloon *et al.*, 1988; Hirose & Kushiro, 1993; Baker & Stolper, 1994). It is inevitable that erupted MORB melts must inherit some of their major element compositional variability from their parental melts in the mantle, but the variable and elevated FeO values of ~ 7 to 11 wt% in melts with $Mg^{\#} = 0.55–0.68$ cannot be interpreted as indicating pressures of melting and mantle temperature variation of ~ 250 K.

Lecroart *et al.* (1997) attempted to correct for the effects of low-pressure fractionation using FeO/MgO ratios. They found that, in major element oxide ratio–ratio spaces using MgO as the denominator, many MORB suites converge to a common point with $\sim 8\%$ MgO, and thus interpreted this convergence as supporting the premises of the Klein & Langmuir (1987) correction scheme. However, we show that $Mg^{\#}$ varies significantly at $MgO = 8$ wt% (Fig. 6).

Fig. 6. Variation of $Mg_8^\#$ vs Fe_8 (a) and ridge axial depth (b) to demonstrate the error in the concept of the fractionation-correction of Klein & Langmuir (1987) to $MgO = 8\,wt\%$. The error is revealed by calculating $Mg_8^\# = Mg_8/(Mg_8 + Fe_8^{2+})$ (note: 10% total Fe is assumed to be Fe^{3+} in all $Mg^\#$ calculations) using the atomic proportion of Fe_8 and the atomic proportion of $8\,wt\%$ MgO. The significance of Fe_8 is thus conceptually exactly the same as the significance of $Mg_8^\#$. (c) Figure 2b reproduced for comparison with (b).

Correction for fractionation effects to $Mg^\# = 0.72$

Niu *et al.* (1999, 2002) corrected MORB compositions for fractionation effects to a constant $Mg^\#$ value of 0.72, instead of $MgO = 8\,wt\%$. By correcting to $Mg^\# = 0.72$, we still do not recover the primary magmas whose compositions are not precisely known (see Fig. 1). By assuming that mantle melts passing through the Moho must be in equilibrium with olivine of $>Fo_{89}$, then correction of MORB melts for fractionation to $Mg^\# = 0.72$ is justified because a melt with $Mg^\# = 0.72$ is in equilibrium

with olivine of $Fo_{89.6}$ (following Roeder & Emslie, 1970). Furthermore, the most primitive MORB melts sampled have $Mg^\# \sim 0.72$ (not higher), which allows reliable fractionation correction up to this $Mg^\#$ value (see below). C. H. Langmuir (personal communication, 2006) stated 'it does not matter whether the data are corrected to a constant MgO or $Mg^\#$, the meaning is the same and the implication of the corrected results is the same'. It is explicit in both practice and concept that it does matter. Melts corrected for fractionation effect to $Mg^\# = 0.72$ are in equilibrium with mantle olivine of $\geq Fo_{89.6}$, thus reflecting more faithfully mantle signals or processes. In contrast, melts corrected to $MgO = 8\,wt\%$ with $Mg^\# = 0.55 \sim 0.68$ are in equilibrium with more Fe-rich, non-mantle, olivine compositions of $Fo_{79.6-88.1}$ and mainly record cooling-induced fractional crystallization at crustal levels (Fig. 6).

Our correction procedure to minimize the effects of low-pressure differentiation has been discussed previously (Niu *et al.*, 1999, 2002). This is further described in Electronic Appendix A and has been applied to each of the 9130 samples used, and to every major and minor element oxide. As each oxide is corrected independently (other than $Mg^\#$), the sum of Si_{72}, Ti_{72}, Al_{72}, Fe_{72}, Mn_{72}, Mg_{72}, Ca_{72}, Na_{72}, K_{72} and P_{72}, which is $\sim 100\%$ within 'analytical error', suggests the effectiveness of the correction procedure.

Chemistry–depth correlations: Fe_8 and Na_8 are equivalent to fractionation-uncorrected raw data

Figure 7 compares our averages of fractionation-uncorrected data (Table 1 and Fig. 4) with Klein & Langmuir's (1987) fractionation-corrected data (i.e. Fe_8, Na_8 and $Mg^\#$ calculated from Fe_8 and $MgO = 8\%$). The similarity is remarkable. There is no simpler way than Fig. 7 to demonstrate that Klein & Langmuir's (1987) apparently sophisticated fractionation correction procedure does not really correct for fractionation effects, but reproduces the raw data for samples with $MgO > 7\,wt\%$. Thus, Fe_8, which is effectively fractionation-uncorrected FeO, cannot be used to infer pressures and temperatures of mantle melting based on corrections such as in Figs 2 and 6.

Chemistry–depth correlations: averages of fractionation-corrected data

Table 2 gives depth-interval averaged data corrected for fractionation effects to $Mg^\# = 0.72$. The recalculated $Mg^\#$ (from Fe_{72} and Mg_{72}) is constant at 0.713 ± 0.002 (vs varying from 0.55 to ~ 0.68 calculated from Klein & Langmuir's (1987) Fe_8 and $8\,wt\%$ MgO), an internal test that proves that our fractionation correction procedure is effective (Electronic Appendix A and Fig. 8).

Table 2: Ridge depth interval (250 m) averages of global MORB major element data: averages with standard deviations of data corrected for fractionation effect to $Mg^{\#} = 0.72$

Depth interval (m)	n	Depth (m)	1σ	Si_{72}	1σ	Ti_{72}	1σ	Al_{72}	1σ	Fe_{72}	1σ	Mn_{72}	1σ	Mg_{72}	1σ
250–500	27	425	23	50·122	0·325	0·510	0·128	15·899	0·153	8·318	0·174	0·105	0·073	10·323	0·124
500–750	55	633	51	50·215	0·639	0·695	0·139	16·259	0·306	8·426	0·248	0·007	0·026	10·354	0·210
750–1000	68	856	78	50·527	0·766	0·598	0·251	16·014	0·480	8·400	0·274	0·022	0·051	10·359	0·245
1000–1250	71	1084	78	49·858	1·140	0·669	0·312	16·252	0·673	8·392	0·526	0·024	0·053	10·362	0·466
1250–1500	120	1397	83	49·760	0·880	0·892	0·327	16·386	0·595	7·946	0·429	0·049	0·076	10·057	0·347
1500–1750	149	1635	85	49·535	1·213	1·026	0·292	16·678	0·693	8·032	0·386	0·049	0·073	10·119	0·366
1750–2000	278	1904	74	49·408	1·345	0·884	0·241	16·613	0·839	8·161	0·446	0·068	0·073	10·227	0·400
2000–2250	400	2148	79	49·778	0·803	0·991	0·226	16·380	0·531	7·992	0·492	0·055	0·071	10·064	0·446
2250–2500	1060	2402	71	49·593	0·870	0·921	0·202	16·441	0·697	8·217	0·342	0·038	0·066	10·292	0·300
2500–2750	3434	2619	70	49·685	0·299	1·021	0·028	16·272	0·216	8·194	0·078	0·123	0·024	10·260	0·093
2750–3000	817	2873	68	49·691	0·741	1·018	0·212	16·415	0·512	8·186	0·322	0·143	0·028	10·248	0·275
3000–3250	820	3132	74	49·669	0·795	1·064	0·242	16·542	0·537	8·202	0·355	0·148	0·025	10·254	0·282
3250–3500	531	3376	76	49·565	0·731	1·091	0·153	16·696	0·616	8·138	0·326	0·143	0·027	10·204	0·265
3500–3750	346	3625	81	49·836	0·763	1·092	0·155	16·622	0·536	8·008	0·361	0·143	0·021	10·099	0·320
3750–4000	348	3886	71	49·881	0·871	1·140	0·165	16·639	0·516	7·934	0·388	0·143	0·027	10·029	0·361
4000–4250	132	4093	57	49·907	0·683	1·099	0·142	16·392	0·518	7·991	0·425	0·148	0·030	10·070	0·368
4250–4500	238	4431	57	49·666	0·674	1·137	0·134	16·474	0·425	8·075	0·314	0·144	0·040	10·153	0·250
4500–4750	77	4585	44	49·989	0·716	1·080	0·135	16·608	0·329	7·993	0·275	0·141	0·024	10·087	0·227
4750–5000	88	4863	78	49·653	0·716	1·241	0·198	17·072	0·531	7·869	0·413	0·141	0·021	9·973	0·358
5000–5250	31	5113	57	49·986	0·503	1·126	0·195	16·902	0·914	7·502	0·527	0·139	0·021	9·614	0·514
5250–5500	32	5428	19	50·442	0·316	1·212	0·068	17·291	0·278	7·485	0·107	0·161	0·022	9·550	0·101
5500–5750	8	5600	0	49·406	0·214	1·148	0·011	17·694	0·058	7·517	0·070	0·130	0·007	9·616	0·063

Depth interval (m)	Ca_{72}	1σ	Na_{72}	1σ	K_{72}	1σ	P_{72}	1σ	Sum (72)	1σ	$Mg^{\#}$ (72)	1σ	Ca_{72}/Al_{72}	1σ	K_{72}/Ti_{72}	1σ
250–500	12·072	0·265	1·650	0·131	0·056	0·060	0·120	0·037	99·18	0·54	0·711	0·004	0·759	0·016	0·100	0·074
500–750	11·438	0·379	1·648	0·147	0·116	0·042	0·153	0·036	99·31	0·78	0·709	0·005	0·704	0·022	0·158	0·307
750–1000	11·800	0·369	1·747	0·263	0·074	0·147	0·129	0·040	99·67	1·09	0·710	0·005	0·738	0·040	0·092	0·218
1000–1250	11·641	0·617	1·891	0·415	0·092	0·150	0·103	0·048	99·28	1·44	0·710	0·009	0·718	0·054	0·099	0·195
1250–1500	11·546	0·600	2·317	0·525	0·146	0·108	0·129	0·058	99·23	1·11	0·715	0·006	0·706	0·050	0·148	0·300
1500–1750	11·185	0·603	2·406	0·334	0·159	0·149	0·138	0·060	99·33	1·17	0·714	0·006	0·673	0·059	0·160	0·282
1750–2000	11·186	0·612	2·245	0·295	0·168	0·140	0·120	0·066	99·08	0·93	0·713	0·005	0·676	0·059	0·172	0·164
2000–2250	11·308	0·606	2·270	0·323	0·237	0·231	0·159	0·066	99·23	1·29	0·714	0·007	0·691	0·049	0·215	0·233
2250–2500	11·273	0·603	2·198	0·314	0·121	0·127	0·128	0·053	99·22	0·92	0·713	0·005	0·687	0·053	0·127	0·248
2500–2750	11·185	0·154	2·360	0·036	0·113	0·011	0·138	0·011	99·35	0·89	0·713	0·005	0·688	0·032	0·109	0·475
2750–3000	11·037	0·515	2·338	0·320	0·129	0·116	0·151	0·076	99·36	0·92	0·713	0·005	0·673	0·044	0·124	0·244
3000–3250	10·855	0·576	2·411	0·328	0·132	0·091	0·140	0·043	99·42	1·00	0·712	0·006	0·657	0·047	0·122	0·249
3250–3500	10·637	0·501	2·551	0·274	0·126	0·085	0·145	0·039	99·30	0·88	0·713	0·005	0·638	0·043	0·113	0·225
3500–3750	10·576	0·393	2·577	0·259	0·153	0·118	0·144	0·037	99·25	0·96	0·714	0·005	0·637	0·032	0·143	0·226
3750–4000	10·413	0·667	2·736	0·342	0·154	0·156	0·151	0·044	99·22	0·93	0·715	0·005	0·627	0·048	0·134	0·278
4000–4250	10·251	0·536	2·741	0·286	0·118	0·073	0·113	0·030	98·83	0·96	0·714	0·005	0·626	0·037	0·109	0·223
4250–4500	10·450	0·483	2·700	0·237	0·128	0·053	0·132	0·044	99·06	0·95	0·713	0·004	0·635	0·038	0·112	0·210
4500–4750	10·688	0·561	2·532	0·266	0·140	0·071	0·153	0·030	99·41	0·96	0·714	0·004	0·644	0·035	0·127	0·226
4750–5000	9·879	0·651	3·057	0·416	0·151	0·066	0·148	0·040	99·18	0·86	0·715	0·006	0·580	0·050	0·122	0·279
5000–5250	9·800	0·838	3·151	0·654	0·176	0·072	0·083	0·055	98·48	1·01	0·717	0·007	0·584	0·079	0·157	0·265
5250–5500	8·988	0·212	3·573	0·124	0·187	0·022	0·115	0·017	99·00	0·55	0·716	0·001	0·520	0·013	0·155	0·109
5500–5750	8·970	0·086	3·661	0·060	0·155	0·010	0·062	0·021	98·36	0·20	0·717	0·001	0·507	0·004	0·135	0·412
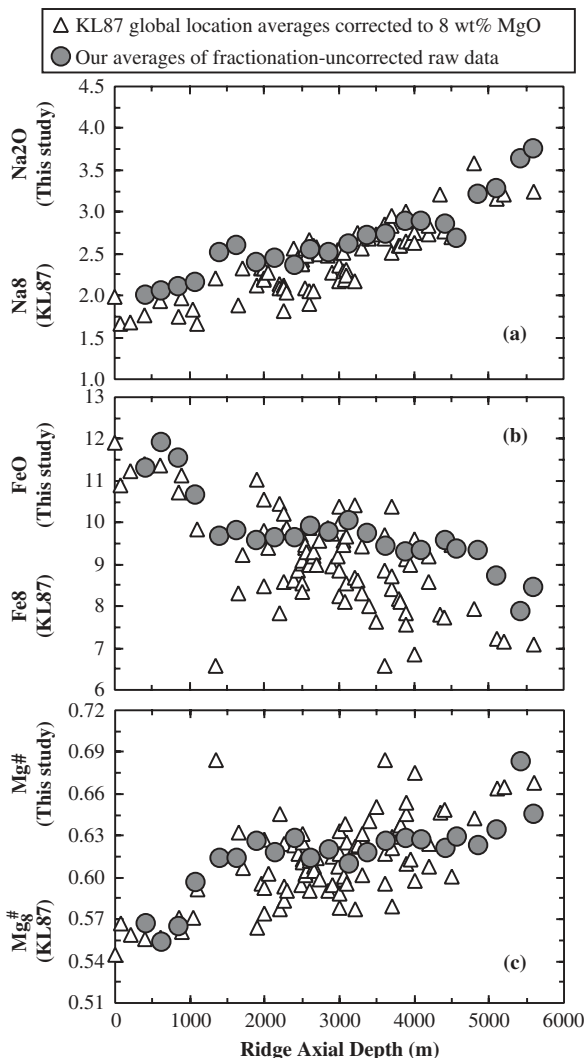
Fig. 7. Comparison of fractionation-uncorrected depth-interval averages (this study) as a function of ridge axial depth with Na_8 (a) and Fe_8 (b) of Klein & Langmuir (1987), and with $Mg_8^\#$ (c) calculated from Klein & Langmuir's (1987) Fe_8 and $MgO = 8\,wt\%$.

Figures 5b and 9 show that the systematics of Ti_{72}, Al_{72}, Fe_{72}, Ca_{72}, Na_{72}, K_{72} and Ca_{72}/Al_{72} with ridge axial depth seen in the fractionation-uncorrected raw data (Figs 4 and 5a) remain, although the abundance levels differ and the degrees of depth dependence vary (see Electronic Appendix B for graphic comparisons). Hence, erupted MORB melts inherit compositional systematics from their parental melts in the mantle. Figure 9a shows parallel Fe_{72}–depth and Mg_{72}–depth trends. That is, there is a clear positive Fe_{72}–Mg_{72} correlation ($Fe_{72} = 1.1256Mg_{72} - 3.331$, $R = 0.989$) (derived from data in Table 2) that exists in model primary melts (Fig. 1) and melts in peridotite melting experiments, but is never seen in actual MORB melts, which are far too evolved.

Chemistry–depth correlations: more on Fe_{72} vs Fe_8 and Na_{72} vs Na_8

Given that the original Klein & Langmuir (1987) concept of Fe_8 and Na_8 has become deeply rooted in the literature, it is necessary to discuss more about Fe_8. Figure 10 compares our Fe_{72} (Fig. 10a) with Fe_8 by Klein & Langmuir (1987) (Fig. 10b) plotted against ridge axial depth. Both parameters show a progressive increase with decreasing ridge axial depth, but the range of Fe_8 (~ 5.0 Fe units) is five times greater than the range of Fe_{72} (~ 1.0 Fe unit). If the range of Fe_8 corresponds to mantle temperature variation of ~ 250 K beneath global ocean ridges as proposed by Klein & Langmuir (1987), then the small range in Fe_{72}, from 7·5 to 8·5, would suggest only ~ 50 K variation.

We can use Langmuir *et al.*'s (1992) equation (29) ($P_{o[solidus]} = 6.11Fe_8 - 34.5$; $T_{o[solidus]} = 1150 + 13P_o$) to calculate P_o and T_o. For Klein & Langmuir's (1987) Fe_8 range of 6·5–11·5 (Fig. 10b), we obtain $P_o = 5.2$–35·8 kbar and $T_o = 1218$–1615°C or $T_P = 1208$–1551°C by using an adiabatic gradient of 1·8°C/kbar (McKenzie & Bickle, 1988). It should be noted that a range of adiabat values (from 1·0 to 1·8°C/kbar) have been used by others (e.g. Langmuir *et al.*, 1992; Turcotte & Phipps Morgan, 1992; Fang & Niu, 2003), but the exact value is not critical as we are interested in temperature variation ranges, although the ΔT_P value (converted from ΔT_o) is greater for a smaller adiabat value. The Langmuir *et al.* (1992) data suggest that there is a huge mantle potential temperature variation of $\Delta T_P = 1551°C$–1208°C = 342 K beneath global ocean ridges, which is actually greater than Klein & Langmuir's (1987) preferred $\Delta T_P = 250$ K. More conservatively, if we use $Fe_8 = 7$–11 (Fig. 10), we obtain $P_o = 8.3$–32·7 kbar, $T_o = 1258$–1575°C (i.e. $T_P = 1243$–1516°C) or $\Delta T_P = 274$ K, which is still greater than, but similar to, Klein & Langmuir's (1987) preferred $\Delta T_P = 250$ K. On the other hand, if we use $Fe_{72} = 7.5$–8·5 (Fig. 10a), we obtain $P_o = 11.3$–17·4 kbar, $T_o = 1297$–1377°C (i.e. $T_P = 1277$–1345°C) or $\Delta T_P = 68$ K.

Two points should be noted from this exercise: (1) as we use samples from the deepest ridges such as the Cayman Rise (~ 5500 m) and the shallowest ridges such as the Reykjanes Ridge (~ 500 m), and if Fe_{72} indeed has pressure significance (see below), then the mantle potential temperature variation would be $\Delta T_P \sim 70$ K, rather than $\Delta T_P = 250$ K (Klein & Langmuir, 1987; Langmuir *et al.*, 1992) beneath global ocean ridges; (2) interestingly, the MORB mantle $T_P = 1277$–1345°C based on Fe_{72} is similar to the value of ~ 1280°C recommended by McKenzie & Bickle (1988) or the new estimate of 1315°C (D. McKenzie, personal communication, 2006) or 1350°C as suggested by Fang & Niu (2003).

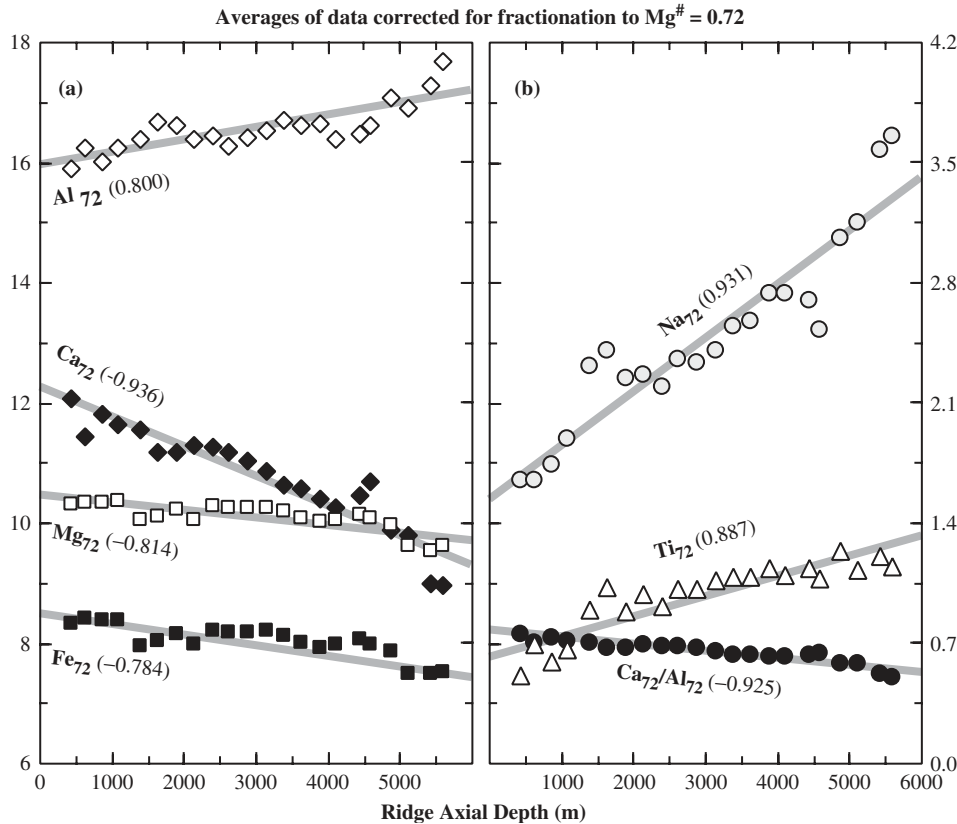Figure 11 shows Klein & Langmuir's (1987) inverse Na_8–Fe_8 trend, which they call a global trend (Klein & Langmuir, 1989) and is interpreted as indicating mantle temperature control on pressures (depths) and extents of

melting. That is, a hotter mantle rises and intersects the solidus at a greater depth (high Fe_8), has a taller melting column, and thus melts more (lower Na_8) than a cooler mantle. Langmuir *et al.* (1992) successfully modeled this


Fig. 8. Variation of $Mg^\#$ vs ridge axial depth showing that the correction procedure to $Mg^\# = 0.72$ is effective. $Mg^\#$ was recalculated after FeO and MgO were corrected to Fe_{72} and Mg_{72} for each of the 9130 samples before obtaining the depth-interval averages (Table 2); the $Mg^\# = 0.713 \pm 0.002$ for $n = 9130$ is close to 0.72, but contrasts with the $Mg_8^\#$ range of 0.55–0.68 calculated from Klein & Langmuir's (1987) Fe_8 and MgO = 8 wt%.

'global trend' by accumulated fractional melting as a result of increasing T_P (increasing P_o) from beneath deep ridges to beneath shallow ridges (see Langmuir *et al.*, 1992, fig. 53). Figure 11 compares Klein & Langmuir's (1987) Na_8–Fe_8 with Na_{72}–Fe_{72}, for which both 9130 data points and depth interval averages (Figs 3, 7 and 9) are plotted. Explicitly, by using Fe_8, Klein & Langmuir (1987) overestimated the ranges of melting pressures towards higher values. It should be noted that a significant inverse Na_{72}–Fe_{72} trend is well defined by the depth-interval averaged data (Fig. 11b). The Na_8–Fe_8 'global trend' (Fig. 11a) was modeled by accumulated fractional melting by Langmuir *et al.* (1992); however, the Na_{72}–Fe_{72} trend (Fig. 11b) cannot be modeled by the same process as this would require changes in all possible parameters (e.g. *P, T*, mode and style of melting, source mineralogies and relevant partition coefficients). The relevant question is if the small Fe_{72} variation (1·0 Fe unit) defined by depth-interval averages on a global scale (Figs 9–11) has any significance at all in terms of pressures of melting. If so, how much might the pressure difference be, and if it is pressure-independent, what could cause the small Fe_{72} variation, the inverse Na_{72}–Fe_{72} correlation, and all the oxide–depth correlations prominent in both fractionation-uncorrected and -corrected data (Figs 4, 5, 7, 9 and 10).

Fig. 9. Plots of ridge-depth interval averages of fractionation-corrected (to $Mg^\# = 0.72$) major element oxides as a function of ridge axial depth (see Table 2, and Electronic Appendices A and B for details). (a) Al_{72}, Ca_{72}, Mg_{72}, Fe_{72}; (b) Na_{72}, Ti_{72}, Ca_{72}/Al_{72}.
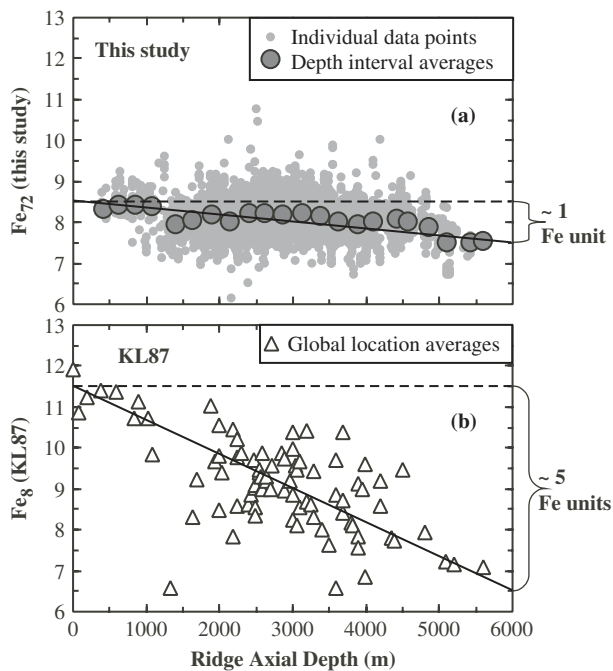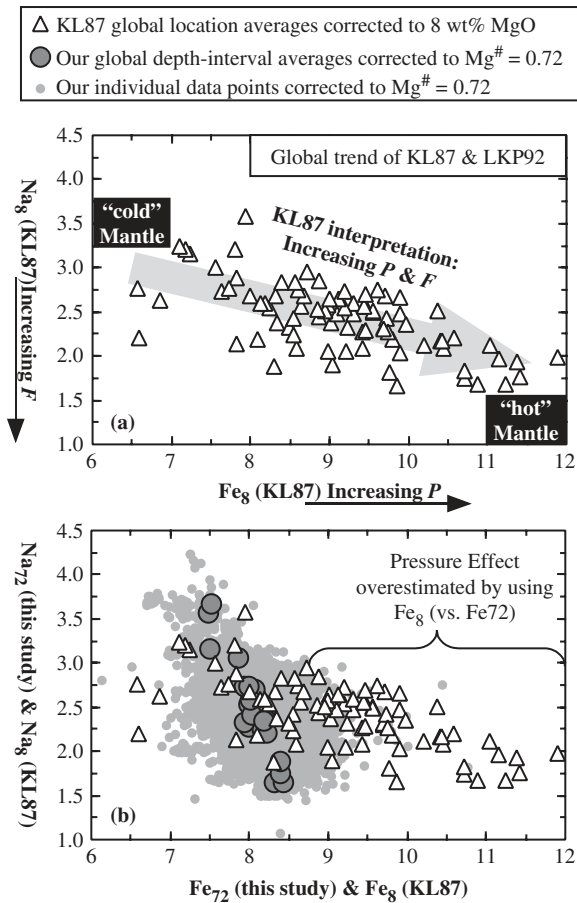
Fig. 10. Comparison of fractionation-corrected FeO expressed as Fe_{72} (this study) (a) and as Fe_8 by Klein & Langmuir (1987) (b) plotted against ridge axial depth to show that the range of Fe_8 is five times greater than that of Fe_{72}. As Klein & Langmuir's (1987) Fe_8 is linearly proportional to initial depth of melting (P_o) and solidus temperature (T_o), and if the Fe_8 variation on a global scale is equivalent to a mantle potential temperature variation of $\Delta T_P = 250$ K, then the small Fe_{72} range would give $\Delta T_P = \sim 50$ K, although none of these calculated Δ_P values are constrained.


Fig. 11. (a) The global trend of Klein & Langmuir (1987) defined by Na_8 vs Fe_8 [$Na_8 = -0.36Fe_8 + 6.26$; equation (28) of Langmuir *et al.* (1992) (LKP92)] with their interpretations indicated. (b) Comparison of the Na_8–Fe_8 global trend with Na_{72}–Fe_{72} for data points of 9130 samples as well as depth-interval averages (Figs 3, 9 and 10).

The small Fe_{72} variation might have no pressure significance

Figures 1 and 12a show explicitly that SiO_2 in primary melts is as sensitive as FeO to the pressure of peridotite melting; FeO increases whereas SiO_2 decreases with increasing melting pressure in the range of 5–30 kbar. Hence, if fractionation-corrected MORB melts preserve the chemical signature of melting pressures, a significant inverse Si_{72}–Fe_{72} trend should exist.

However, this is not the case as shown in Fig. 12b; neither individual data points of the 9130 samples nor averages define any significant trend. Figure 12c shows that the data span a large Si_{72} range at a given ridge axial depth, but do not vary in any systematic way as a function of ridge axial depth as illustrated by the averages. It is likely that MORB melts do preserve signals of melting pressures, and that the large Fe_{72} (Figs 10 and 11) and Si_{72} variations (Fig. 12) displayed by individual data points could partly result from varying depths of melting. However, without first-order Si_{72} decrease, but with only a small Fe_{72} increase, towards shallow ridges, it is unconvincing that mantle melting depth (P_o, thus T_o) increases with decreasing ridge axial

depth (Fig. 12c). This means that the small Fe_{72} variation (1.0 Fe unit) with ridge axial depth (Fig. 10a) might have a different origin (see below).

GLOBAL RIDGE AXIAL DEPTH VARIATION—THE FUNDAMENTAL CONSTRAINT

Mantle potential temperature variation (ΔT_P), plate spreading rate variation (ΔR_{SR}) and mantle source compositional variation (ΔX_{MS}) are the three major variables that determine the extent of mantle melting and MORB compositions (e.g. Niu *et al.*, 2001; Niu, 2004). Of these, ΔR_{SR} can be directly observed, but both ΔT_P and ΔX_{MS} must be inferred. The global ocean ridge axial depth variation (ΔD_{RA}) is not a governing variable, but a physical consequence of mantle processes. The lack of apparent
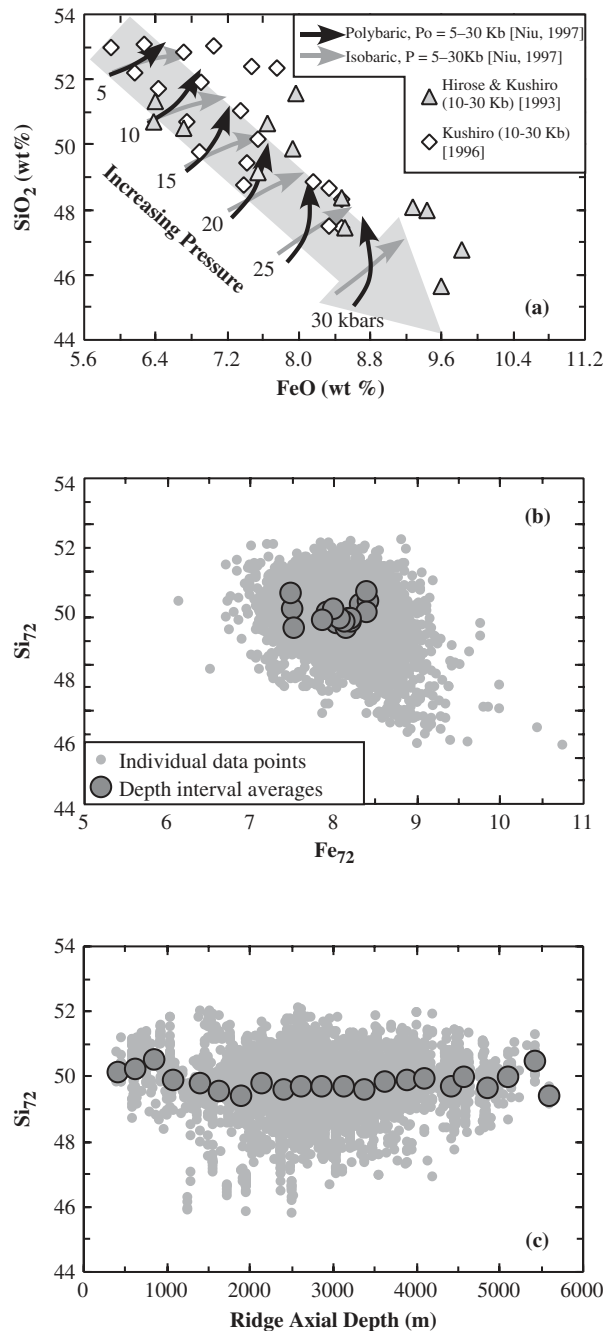
Fig. 12. (a) Variation of wt% SiO_2 vs wt% FeO for model primary melts from Fig. 1 and Niu (1997) (arrowed curves represent increasing extent of melting from 5 to 20%) together with peridotite melting experiments performed under 10–30 kbar pressures (Hirose & Kushiro, 1993; Kushiro, 1996) to show that SiO_2 is as sensitive as FeO to pressure in primary peridotite melts. SiO_2 decreases whereas FeO increases with increasing melting pressure. The scatter results from different source (starting material) compositions and varying extents of melting, but the inverse trend is significant. (b) Si_{72} vs Fe_{72} for 9130 samples and depth-interval averages (from Table 2), showing no trend, but a cluster. (c) Si_{72} values of both 9130 samples and averages vs ridge axial depth. Si_{72} values vary significantly at a given ridge axial depth, and the 'trend' defined by the averages has a slope of ~0; that is, there is no meaningful Si_{72}–ridge axial depth correlation.

correlation between ΔR_{SR} and ΔD_{RA} (Niu & Hékinian, 1997a; Sinton & Rubin, 2007) suggests that ΔD_{RA} is independent of ΔR_{SR}. Therefore, $\Delta D_{RA} = f(\Delta T_P \quad \Delta X_{MS})$ should be true. This reasoning is logical because ΔD_{RA} must be caused by sub-ridge material density variation, and the latter must result from either ΔT_P or ΔX_{MS} or perhaps both. Our task is thus to evaluate the possible contributions of ΔT_P and ΔX_{MS} to ΔD_{RA} by carrying out some simple tests, recognizing the significant correlations of ΔD_{RA} with global MORB compositional variations (ΔX_{MORB}; Figs 4, 5, 7, 9 and 10). It is noteworthy that the ΔD_{RA} in question (i.e. Figs 4, 5, 7, 9 and 10) contains no contribution from 'dynamic topography' because the latter (1) is of local or regional origin, (2) should be removed by the averaging with respect to sample depth regardless of geographical location (Fig. 3), and (3) should not correlate with ΔX_{MORB} on a global scale.

Significance of mantle potential temperature variation

The Klein & Langmuir (1987) and Langmuir et al. (1992) interpretation and current views

We have demonstrated above that it is invalid to use Fe_8 to infer melting pressures or initial depths of melting (Figs 6, 7, 8, 10 and 11). Hence, the Klein & Langmuir (1987) [and Langmuir *et al.* (1992)] interpretation of a global mantle potential temperature variation of $\Delta T_P = 250 \, K$ beneath mid-ocean ridges needs revising. The association of low Na_8 with shallower ridge depths could be consistent with a higher extent of melting (Fig. 7a), and thus higher T_P. We must emphasize, however, that Fe_8 correlates with Na_8 and ridge axial depth (Figs 2 and 7), and this is in fact the essence of the Klein & Langmuir (1987) and Langmuir *et al.* (1992) theory [see Klein & Langmuir, 1987, fig. 12; Langmuir *et al.*, 1992, fig. 53 and equation (29)].

The thickness of melt or magmatic crust (vs crust interpreted from seismic data) produced is predicted to vary with T_P (Klein & Langmuir, 1987; McKenzie & Bickle, 1988; Langmuir *et al.*, 1992) provided that the mantle source composition is uniform, that the effect of spreading rate variation is small, and that melt extraction from the mantle is complete (Niu, 1997; Niu *et al.*, 2001). However, determination of crustal thickness is not a straightforward observation, but an interpretation based on seismic velocity data (White *et al.*, 1992, 2001). In addition, whether the interpreted thickness of the seismic crust represents magmatic crust or not remains debatable (Hess, 1962; Christensen, 1972; Forsyth, 1992; Detrick *et al.*, 1994; Cannat, 1996; Niu, 1997; Niu & Hékinian, 1997a, 1997b; White *et al.*, 2001). We consider that the thickness of seismic crust could be used as a reference, but prefer to use straightforward observations such as ridge axial depth variation as a constraint in evaluating models of mantle processes.

McKenzie & Bickle (1988) originally argued for $T_P = 1280°C$ for normal sub-ridge mantle; $T_P = 1315°C$ is now considered more reasonable (D. McKenzie, personal communication, 2006). 'Because the thickness of the oceanic crust varies very little, most of the upper mantle apart from hot rising jets (plumes) must have approximately the same temperature' (McKenzie & Bickle, 1988, p. 641), implying that $\Delta T_P \approx 0$ (or negligible) beneath global ocean ridges. Shen & Forsyth (1995) argued for $\Delta T_P \leq 60$ K and that the $\Delta T_P = 250$ K of Klein & Langmuir (1987) and Langmuir et al. (1992) was an artifact from mantle heterogeneity. Presnall et al. (2002) argued for $\Delta T_P \approx 20$ K ($T_P = 1240 \pm 10°C$) and that the $\Delta T_P = 250$ K of Klein & Langmuir (1987) and Langmuir et al. (1992) resulted from the effects of source heterogeneity, such as CO_2 content that affects FeO in the melt and thus Fe_8. Herzberg et al. (2007) argued for $\Delta T_P = 1400 - 1280°C = 120$ K based on petrological modeling. If we use Fe_{72} from equation (29) of Langmuir et al. (1992), we would obtain $\Delta T_P < 70$ K (68 K; see above). The range of estimated $\Delta T_P = \sim 0$ K, 20 K, ≤ 60 K, ≤ 70 K, ~ 120 K, ~ 250 K is clearly rather large. All the above researchers have their own reasons why they prefer a particular value or values, but these are not always clear. McKenzie & Bickle (1988) argued for uniform T_P (or $\Delta T_P \approx 0$) because of (1) 'the absence of any pressure effect' (p. 642) in MORB melts, and (2) the uniform thickness of seismic crust beneath normal ocean ridges (excluding Iceland). Klein & Langmuir (1987) and Langmuir et al. (1992) insisted on $\Delta T_P = 250$ K because of (1) the large variation in the thickness of seismic crust, including both Iceland and the Cayman Rise, and (2) the need to explain the large range of Fe_8.

One may argue that Klein & Langmuir (1987) and Langmuir et al. (1992) are consistent with other models for 'normal ocean ridges' with $\Delta T_P < 100$ K if Iceland is excluded. However, this is not the case. Even if samples from shallow ridges (<2000 m deep) are excluded, Fe_8 still has a large range from 7 to 10·5 (see Fig. 6), which would mean $\Delta T_P = 240$ K (i.e. $T_o = 1258-1482°C$ and $T_P = 1243-1482°C$). So, $\Delta T_P = 250$ K by Klein & Langmuir (1987) and Langmuir et al. (1992) refers to normal ocean ridges unaffected by hotspots or mantle plumes (e.g. Iceland) on a global scale. Adopting the same approach using Fe_{72} and samples from ridges >2000 m deep gives $Fe_{72} = 7·5-8·1$, and $\Delta T_P = 41$ K.

All these simple exercises tell us that the large $\Delta T_P = 250$ K variation proposed by Klein & Langmuir (1987) and Langmuir et al. (1992) cannot be because the dataset includes hotspots (e.g. Iceland) and hotspot-influenced ridges (e.g. Reykjanes Ridge), but because of using Fe_8, which led them to reach erroneous conclusions (Figs 6, 7, 8, 10 and 11). We still do not know precisely what ΔT_P is beneath the global ocean ridge system, but (1) if we take into account some robust aspects of the arguments by other workers (e.g. McKenzie & Bickle, 1988; Shen & Forsyth, 1995; Presnall et al., 2002; Herzberg et al., 2007), and (2) if we assume $\Delta T_P = 68$ K (based on Fe_{72}; see above) using a dataset that considers all ridges including the Reykjanes Ridge, then we can say with confidence that ΔT_P is likely to be $\ll 100$ K. As this latter statement assumes that Fe_{72} has pressure significance that is actually unsupported by the data (i.e. lack of inverse Si_{72}–Fe_{72} correlation and lack of Si_{72} systematics with ridge axial depth; Fig. 12), there is no convincing evidence to argue for $\Delta T_P > 50$ K beneath global ocean ridges.

The rapidity of thermal diffusion also does not favor the development of large lateral thermal gradients in the shallow mantle that could persist in time and space. More importantly, the seismic low-velocity zone (LVZ), which corresponds to a low-viscosity zone (lvz) at about 100 to ~ 250 km depth in the mantle continuous beneath global ocean ridges (Phipps Morgan et al., 1995; Ekström & Dziewonski, 1998), is arguably the most dynamic region in the upper mantle in terms of vigor in convection and scales of lateral flow (Phipps Morgan et al., 1995; Niu et al., 1999; Niu & Hékinian, 2004; Niu, 2005). Hence, the LVZ processes would diminish, not create or enhance, temperature variation, if any, beneath ocean ridges.

We foresee that a more precise and definitive estimate of ΔT_P beneath ocean ridges will be possible when we seriously consider mantle compositional variations on local, regional and global scales (e.g. Natland, 1989; Albarède, 1992; Langmuir et al., 1992; Niu & Batiza, 1994, 1997; Niu et al., 1996, 1999, 2001, 2002; Niu, 1997, 2004; Castillo et al., 1998, 2000). We emphasize the effect of major element compositional variation, not minor incompatible elements such as K_2O (Shen & Forsyth, 1995) or CO_2 (Presnall et al., 2002) because it is not obvious how K_2O and CO_2 variations could explain the ~ 5000 m ocean ridge axial depth variation. Comparison of MORB melts with hotspot melts can help to evaluate MORB mantle T_P and ΔT_P (e.g. McKenzie & Bickle, 1988; Herzberg & O'Hara, 2002). However, Green et al. (2001) and Green & Falloon (2005) have argued that $T_P = 1430°C$ for both MORB mantle and hotspot mantle such as that beneath Hawaii. These workers emphasize that it is not T_P variation, but mantle compositional heterogeneity as a byproduct of plate tectonics that is responsible for the diverse range of intraplate hotspot and MORB magmas.

So, what is the actual contribution of ΔT_P to the range of axial depths of the global ridge system ($\Delta D_{RA} = 5$ km)? We do not know, but it is likely to be very small because we have shown above that ΔT_P is likely to be ≤ 50 K beneath ocean ridges. Additionally, there are some fairly robust arguments that can be made on the basis of some straightforward physics.
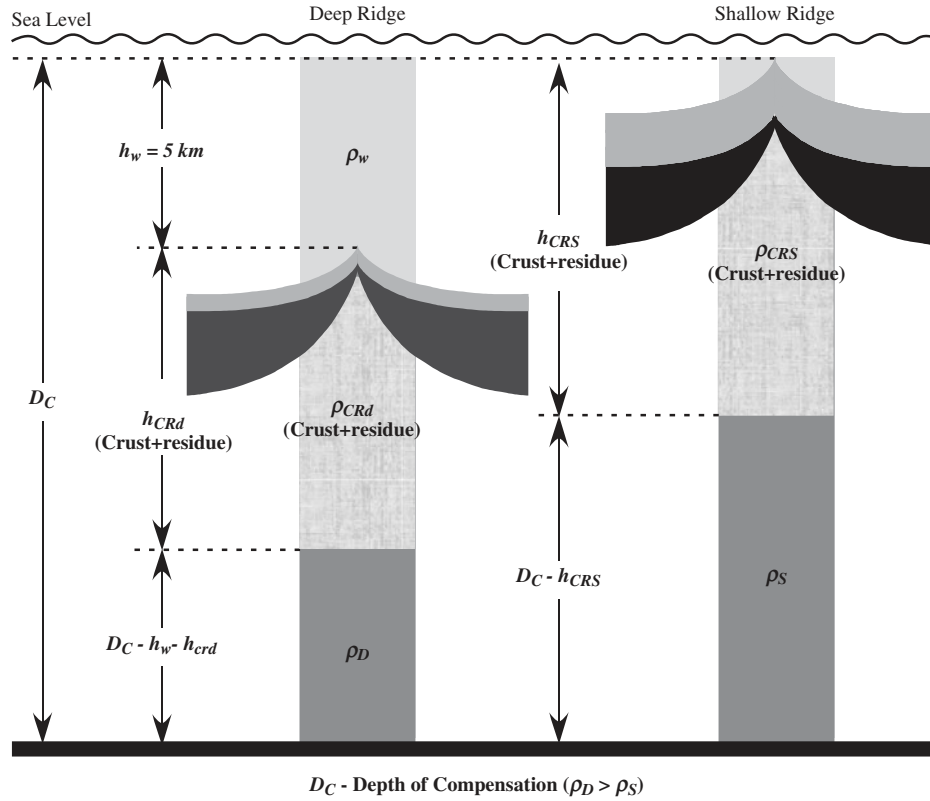
Fig. 13. Schematic illustration, not to scale, showing that the principles of the 'Pratt isostasy' can be used to explore what might cause the ~5 km global ocean ridge axial relief (i.e. $\Delta D_{RA} = h_W = 5$ km). As the global ocean ridge axial depth variation is a continuum (Figs 3–5 and 7–10), by comparing the deepest (e.g. the ~5·5 km deep Cayman Rise) and shallowest (e.g. the ~0·5 km deep Reykjanes Ridge) end-member ridges, we consider a global ridge axial depth variation of ~5000 m. Whether the ridge is shallow (S, subscript) or deep (D, subscript), the mass in these two columns above a common compensation depth (D_C) must be the same as described by equations given in the text. The crust is assumed to be ~3 km thick beneath the deep ridge (e.g. the Cayman Rise) and ~9 km beneath the shallow ridge (e.g. the Reykjanes Ridge) following Klein & Langmuir (1987), resulting from ~5% melting and ~15% melting, respectively, calculated using the Niu (1997) model and the Ca_{72}/Al_{72} ratios (Fig. 9). We further assume (1) $\rho_{Crust} = 2·85$ g/cm^3, (2) $\rho_D = 3·35$ g/cm^3 for the fertile mantle density beneath the deep ridge with a varying fertile mantle ρ_S ($<\rho_D$) beneath the shallow ridge, whose value decreases by increasing temperature to evaluate the effect of ΔT_P on $\Delta\rho$, and thus on D_C, to explain the $\Delta D_{RA} = 5$ km, (3) ~60 km high column of melting residues, and (4) the density of residues reduced by 0·22% (i.e. 0·22% of ρ_D, maximum value) by 5% melt extraction beneath the deep ridge, and by 0·69% (i.e. 0·69% of ρ_S, maximum value) by 15% melt extraction beneath the shallow ridge using DENSCAL (Niu & Batiza, 1991b, 1991c). It should be noted that the density values are mean values for all relevant layers. (See Electronic Appendix C for calculation details.)

Contribution of ΔT_P to ΔD_{RA}: a simple isostasy test

In this section, we examine whether any possible ΔT_P can explain the axial ridge depth difference $\Delta D_{RA} = 5$ km between two end-member ridges (i.e. deep ridge, D_{Water} ~5500 m at the Cayman Rise; shallow ridge, D_{Water} ~500 m at the Reykjanes Ridge), which encompass the 5 km ridge axial depth variation on a global scale (Figs 3–10). Of the two isostasy hypotheses (i.e. 'Airy isostasy' and 'Pratt isostasy'), 'Pratt isostasy' is relevant to ocean ridges because there is no 'mountain root' involved. As the effect of dynamic topography, by the very nature of our averaging process, is removed in the chemistry–depth relationships (Figs 4, 5, 7, 9 and 10), the straight-forward physics is that ridge axial depth variation must be determined by sub-ridge material density variation whether the latter is caused by temperature variation or compositional variation or both.

Figure 13 shows that whether the ridge is shallow or deep, the mass between the two columns above the common compensation depth (D_C) must be the same as described by the equation

$$h_{CRS}\rho_{CRS} + (D_C - h_{CRS})\rho_S = h_W\rho_W + h_{CRD}\rho_{CRD} - (D_C - h_W - h_{CRD})\rho_D.$$

The equation

$$D_C = \frac{h_W\rho_W + h_{CRD}\rho_{CRD} - (h_W + h_{CRD})\rho_D - h_{CRS}\rho_{CRS} + h_{CRS}\rho_S}{(\rho_S - \rho_D)}$$

is derived to calculate the compensation depth. It should be noted that in the Pratt isostasy model, D_C is the minimum common depth above which the mass in the two columns is the same. The mass in the two columns is

always the same above any depth $>D_C$ in terms of mass contributions to the surface topography. To explain the $\Delta D_{RA} = 5$ km variation between the two end-member ridges, we need to consider the sub-ridge density contributions of the crust, the residual mantle (after MORB melt extraction) and the fertile mantle as described in the caption to Fig. 13 and detailed in Electronic Appendix C. Consideration of (1) crustal thickness variation (e.g. from ~3 km beneath deep ridges such as the Cayman Rise to ~9 km beneath shallow ridges such as the Reykjanes Ridge) and (2) residual mantle density variation as a result of melt extraction (less depleted and less buoyant residues beneath deep ridges and more depleted and more buoyant residues beneath shallow ridges) (Fig. 13) is inadequate to explain the $\Delta D_{RA} = 5$ km. We thus evaluate the additional effect of reducing the density ρ_S by increasing mantle temperature beneath the shallow ridge relative to the deep ridge. Figure 14a shows density reduction (%) with increasing temperature by using a volume thermal expansion coefficient of $\alpha = 3 \times 10^{-5}$/K. The solid curves in Fig. 14b and c, which already consider the effect of crustal and residual mantle density variation (see Electronic Appendix C for details), show that to explain the $\Delta D_{RA} = 5$ km, how D_C changes in response to density reduction (%) beneath the shallow ridge relative to beneath the deep ridge as a result of temperature variation.

We consider two scenarios following the conclusions of Klein & Langmuir (1987), assuming: (1) $\Delta T_P = 250$ K and (2) $D_C = 150–200$ km.

Scenario 1. For $\Delta T_P = 250$ K (labeled [1] in Fig. 14a and c), which has an effect in density reduction of 0·75% (labeled [2] and [3] in Fig. 14a and b), $D_C = 380$ km (labeled [4] in Fig. 14b and c). That is, the ~380 km long mantle column beneath the shallow ridge must be 250 K hotter than the ~375 km long (= 380 km − 5 km water column) mantle column beneath the deep ridge. This temperature variation requires continuous (vs discrete) T_P increase from beneath deep ridges to beneath shallow ridges by 250 K in the ~upper 380 km of the mantle to explain the systematically correlated variations of MORB chemistry with ridge axial depth on a global scale (Figs 4, 5, 7, 9 and 10). It is physically not straightforward how $\Delta T_P = 250$ K could persist in time and space in the upper ~380 km of the mantle beneath global ocean ridges, which is dynamically the most vigorous portion of the mantle.

Scenario 2. For $D_C = 200$ km (or 150 km) (labeled [5] and [6] in Fig. 14), it requires a density reduction of 1·78% (or 2·88% if $D_C = 150$ km). This requires the 200 km long (or 150 km if $D_C = 150$ km) mantle column beneath the shallow ridge be 594 K (or 961 K if $D_C = 150$ km) hotter than the 195 km (or 145 km if $D_C = 150$ km) mantle column beneath the deep ridge. This is physically improbable. Such temperature difference (i.e. 594 K or
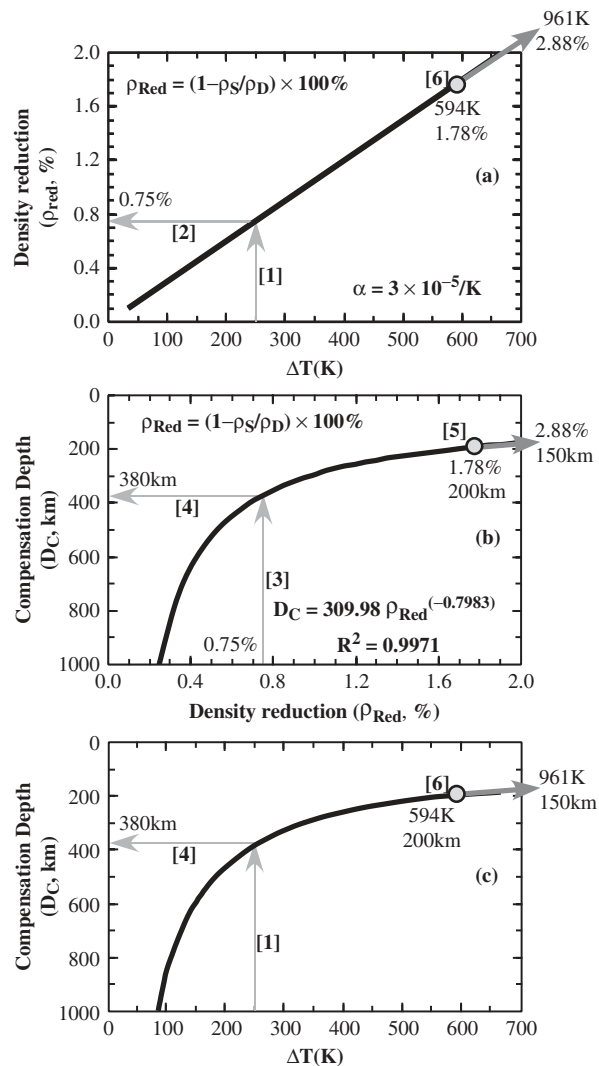
Fig. 14. Model results based on Fig. 13 showing mantle density and isostatic compensation depth (D_C) variations as a function of mantle temperature variation after considering the effects of variation in the thickness of buoyant crust and relatively buoyant residual mantle because of melt extraction, which is inadequate to explain the $\Delta D_{RA} = 5$ km (see Electronic Appendix C for details). (a) The effect of temperature variation (ΔT) on the density of mantle rocks. (b) and (c) show that, to explain the $\Delta D_{RA} = 5$ km (= h_W in Fig. 13), the required mantle compensation depth (D_C) varies as a function of temperature variation (i.e. T_B increase beneath the shallow ridge relative to beneath the deep ridge) induced density variation [see (a)]. (See text and Electronic Appendix C for details of labels 1, 2, 3, 4, 5 and 6.).

961 K) is equivalent to or greater than the negative thermal buoyancy required for oceanic lithosphere subduction.

The above two scenarios are different expressions of the same theory of Klein & Langmuir (1987) and Langmuir *et al.* (1992). If either scenario fails, both scenarios fail. We thus cannot avoid the conclusion that $\Delta T_P = 250$ K is inconsistent with $D_C = 150–200$ km.

Consideration of sub-ridge density variation as a result of (1) crustal thickness variation and residual mantle density variation as well as $\Delta T_P = 250$ K cannot explain the $\Delta D_{RA} = 5$ km unless $D_C > 380$ km (vs 150–200 km) (Fig. 14). More realistically, if we consider $\Delta T_P < 100$ K (i.e. $<0.30\%$ density reduction), then D_C must be >847 km, which makes it more difficult to explain the observations. The situation would be even more difficult if $\Delta T_P < 50$ K (i.e. $<0.15\%$ density reduction), because a D_C of >1625 km would be required. The straightforward conclusion is that mantle potential temperature variation is incapable of explaining the $\Delta D_{RA} = 5$ km because of the rather small volume thermal expansion coefficient of $\alpha = 3 \times 10^{-5}$/K.

The $\Delta D_{RA} = 5$ km could be explained with $D_C = 150$–200 km if the crust at the Reykjanes Ridge (not Iceland) were >26 km thick. However, a crustal thickness of ~ 9 km (Klein & Langmuir, 1987; Langmuir *et al.*, 1992), not 26 km, is inferred from the available seismic data. Furthermore, a systematic crustal thickness increase from deep ridges to shallow ridges [i.e. crustal thickness (km) $= -4.6 \times$ ridge depth (km) $+ 28.3$] would be required to explain MORB chemistry (Figs 4, 5, 7, 9 and 10), which has not been observed.

Significance of mantle compositional variation

The fundamental concept

The significant correlations of ridge axial depth with fractionation-uncorrected (Figs 4 and 5a) and fractionation-corrected (Figs 5b and 9) MORB major element data are striking. These correlations suggest that both ΔD_{RA} and ΔX_{MORB} are consequences of a common process. We argue above that $\Delta D_{RA} = f(\Delta T_B \ \Delta X_{MS})$ should be true, and we have also demonstrated that ΔT_P is inadequate to explain $\Delta D_{RA} = 5$ km on a global scale. It follows that fertile mantle compositional variation, ΔX_{MS}, is the best candidate to cause $\Delta D_{RA} = 5$ km as well as MORB chemistry. As it is the major elements that determine the phase equilibria, mineralogy, lithology, and physical properties of the rock (trace elements and isotopes are often, but not always, decoupled from major elements; see Niu *et al.*, 1996, 1999, 2001, 2002), we emphasize the importance of major element compositional variation. The global variation in mantle potential temperature, ΔT_B has been inferred from ridge axial depth (assumed thermal buoyancy and thickness of the buoyant crust) and MORB chemistry based on parameters such as Fe_8 and Na_8 (Klein & Langmuir, 1987; Langmuir *et al.*, 1992). In fact, ΔX_{MS} can be inferred from the same observations—ridge axial depth (buoyancy as a result of mantle compositional variation) and MORB composition, which is, to a large extent, inherited from its

mantle source although magma generation processes tend to modify the source signals.

MORB chemistry allows us to infer both magma generation–differentiation processes and sources. The common perception of 'processes vs sources' (or vice versa) is somewhat misleading, tends to focus on one or the other, and, as a result, conceptually neglects the fundamental controls of mantle compositional variation on melt generation 'processes'. It is generally accepted that ΔT_P determines the initial depth and extent of melting, melt production and melt composition, and is reluctantly accepted that ΔR_{SR} determines the depth of melting cessation, thus the extent of melting, melt production and composition, but the role of ΔX_{MS} as driving force for magma generation processes has been largely neglected. The correlations of MORB chemistry with ridge axial depth (Figs 4, 5, 7, 9 and 10) could be explained by ΔT_P and ΔX_{MS}, yet petrologists often choose to favor ΔT_B assuming that $\Delta X_{MS} = 0$ (i.e. there is a uniform mantle source composition for MORB).

Mantle compositional variation, ΔX_{MS}, can (1) cause density variation in the mantle, which in turn (2) controls mantle convection and (3) compensates surface topography, and controls (4) rate of mantle upwelling and decompression melting, (4) extent of melting, (5) melt compositions (both inherited and process-enhanced), and (6) paths of melt evolution. In fact, ΔX_{MS} is much more efficient than ΔT_P in causing mantle density variations (e.g. O'Hara, 1973; Niu & Batiza, 1991b, 1991c; Niu *et al.*, 2003). Given the small volume thermal expansion coefficient of 3×10^{-5}/K, a 1.0% density difference as a result of compositional variation requires a ΔT of 333 K to compensate. We can see from Fig. 14 that if $\Delta T_P < 100$ K, beneath global mid-ocean ridges, we are dealing with less than a 0.3% density difference, which requires $D_C = 847$ km to account for the $\Delta D_{RA} = 5$ km (phase changes are neglected for conceptual clarity). A 0.3% density variation in the upper 847 km of the mantle as a result of compositional variation is physically likely (see below), but it is physically difficult to maintain $\Delta T_P = 100$ K in the upper 847 km of the mantle beneath global ocean ridges in time and space, a model that also requires T_P to increase continuously from beneath deep ridges to beneath shallow ridges. Again, it is physically possible that an $\sim 0.6\%$ density variation may exist beneath ocean ridges as a result of compositional variation above $D_C = 458$ km, but it is physically difficult to maintain $\Delta T_P = 200$ K in the upper 458 km of the mantle beneath global ocean ridges.

Physical consequences of MORB mantle compositional variation

We interpret the significant correlations of ridge axial depth with MORB chemistry on a global scale (Figs 4, 5, 7, 9 and 10) as the result of melting a progressively less

depleted fertile mantle peridotite source from beneath shallow ridges to beneath deep ridges. Figure 15a and b is reproduced from Fig. 9 with only the data regression lines plotted to illustrate the concept. The increase in Al_{72}, Na_{72} and Ti_{72} (also K_{72} in Fig. 5b) and decrease in Ca_{72} and Ca_{72}/Al_{72} in MORB melts with increasing ridge axial depth is consistent with a progressively more enriched (or less depleted) peridotite source (i.e. high Al_2O_3, Na_2O, TiO_2 and K_2O, and low CaO/Al_2O_3). Higher Al_2O_3 ensures a greater amount of modal garnet, and higher Na_2O and Al_2O_3 and lower CaO ensure high jadeite/diopside ratios in the clinopyroxene of the source peridotite below deep ridges. The decrease of Fe_{72} and Mg_{72} in MORB melts with increasing ridge axial depth is also consistent with a more enriched (or less depleted) source peridotite with a lower modal proportion of olivine beneath deep ridges. All these observations are consistent with the fertile MORB mantle source peridotite being not only more enriched (or less depleted) but also denser beneath deep ridges, which explains why they are deep.

Figure 15c shows schematically that ridges are mostly passive features, and that the dense asthenospheric mantle beneath deep ridges should rise more slowly (or 'reluctantly') in response to plate separation. The reduced upwelling rate beneath the deep ridge (1) allows conductive cooling to penetrate to a greater depth, (2) makes the cold thermal boundary layer (CTBL) thicker, (3) causes melting cessation at a deeper level, (4) results in a shorter decompression melting column $(P_o - P_f)$, (5) leads to a lower extent of melting, and (6) to possibly thinner magmatic crust with less depleted (or more enriched) major element compositions at deep ridges than at shallow ridges. Such a physical consequence is conceptually the same as for slow-spreading ridges (see Niu & Hékinian, 1997a, fig. 4). If T_P is the same (i.e. $\Delta T_P \sim 0\,K$) beneath deep and shallow ridges, the solidus would be at a shallower depth beneath the shallow ridge because of the more refractory fertile source (the thick solid line). If T_P is a few tens of degrees hotter beneath shallow ridges, then the solidus would be deeper, perhaps similar to the depth of the solidus beneath the deep ridge (see below and also Electronic Appendix D for detailed discussion).

### Possible systematics of mantle compositional variation beneath global ocean ridges

Fertile mantle composition and its variability cannot be directly observed, but can be modeled (e.g. McDonough & Sun, 1995; see Niu, 1997, for a review), and can also be inferred from the compositions of mantle xenoliths from various tectonic settings, orogenic massif peridotites, abyssal peridotites, ophiolites, etc. Griffin *et al.* (1999) carried out a comprehensive survey of the composition of the sub-continental lithosphere mantle. Figure 16 shows

their 52 average bulk-rock peridotite compositions on MgO variation diagrams. For comparison, the primitive mantle composition of McDonough & Sun (1995) and the model melting residues (0–25% melt extraction) of Niu (1997) are also plotted. As expected, the data are scattered because of the complex histories of these mantle rocks including depletion, refertilization (metasomatism), etc. Nevertheless, the data define SiO_2–MgO, TiO_2–MgO, Al_2O_3–MgO, FeO_t–MgO, CaO–MgO and Na_2O–MgO trends that are all roughly consistent with varying extents of melt depletion. Although most sampled peridotites are expected to be some sort of mantle melting residues, some of the samples are much less depleted and plot towards the primitive mantle composition. Given the known process of plate tectonic recycling (oceanic lithosphere subduction, subcontinental lithosphere 'delamination', etc.), it is reasonable to imagine that these data may reflect or even represent the range of upper mantle compositions beneath ocean ridges, at least the less depleted ones with MgO <41 wt%.

For our purpose, we derive a set of bulk-rock compositional data with varying MgO contents from 37 to 48·5% along the regression lines (the thick grey lines). These derived bulk-rock compositions are used to calculate the modal mineralogy of lower-pressure spinel peridotites and higher-pressure garnet peridotites.

Density of bulk-rocks and constituent minerals as a function of melt depletion under spinel peridotite stability conditions

Figure 17a shows the calculated modes of olivine, opx and cpx (see Niu, 1997, appendix C) as a function of bulk-rock MgO; these resemble the modal systematics of melting residues after varying extents of melt depletion (Niu, 1997). Figure 17b shows calculated mineral density as a function of melt depletion (i.e. increasing MgO) using DENSCAL (Niu & Batiza, 1991b, 1991c). As the isobaric volume thermal expansion coefficients and isothermal compressibilities are very similar for all the silicate minerals of interest, we calculated mineral densities at low pressure and room temperature conditions. We compare density variation as a function of compositional variation (depletion) at the same conditions. Olivine density decreases with increasing extents of melt extraction, which is proportional to bulk-rock MgO (Niu, 1997, fig. 8), and reaches a density reduction (increasing Fo/Fa ratio) of $\sim 1\cdot2\%$ from bulk-rock MgO = 37 to 47·5% (Fig. 17c). Opx density declines by $\sim 0\cdot88\%$, and cpx density declines by 1·6%. However, the bulk-rock density reduction is only 0·66%. This is because olivine has the greatest density throughout (Fig. 17b), and olivine modes increase as the bulk-rock is progressively depleted (Fig. 17a). It is thus conceptually important that although
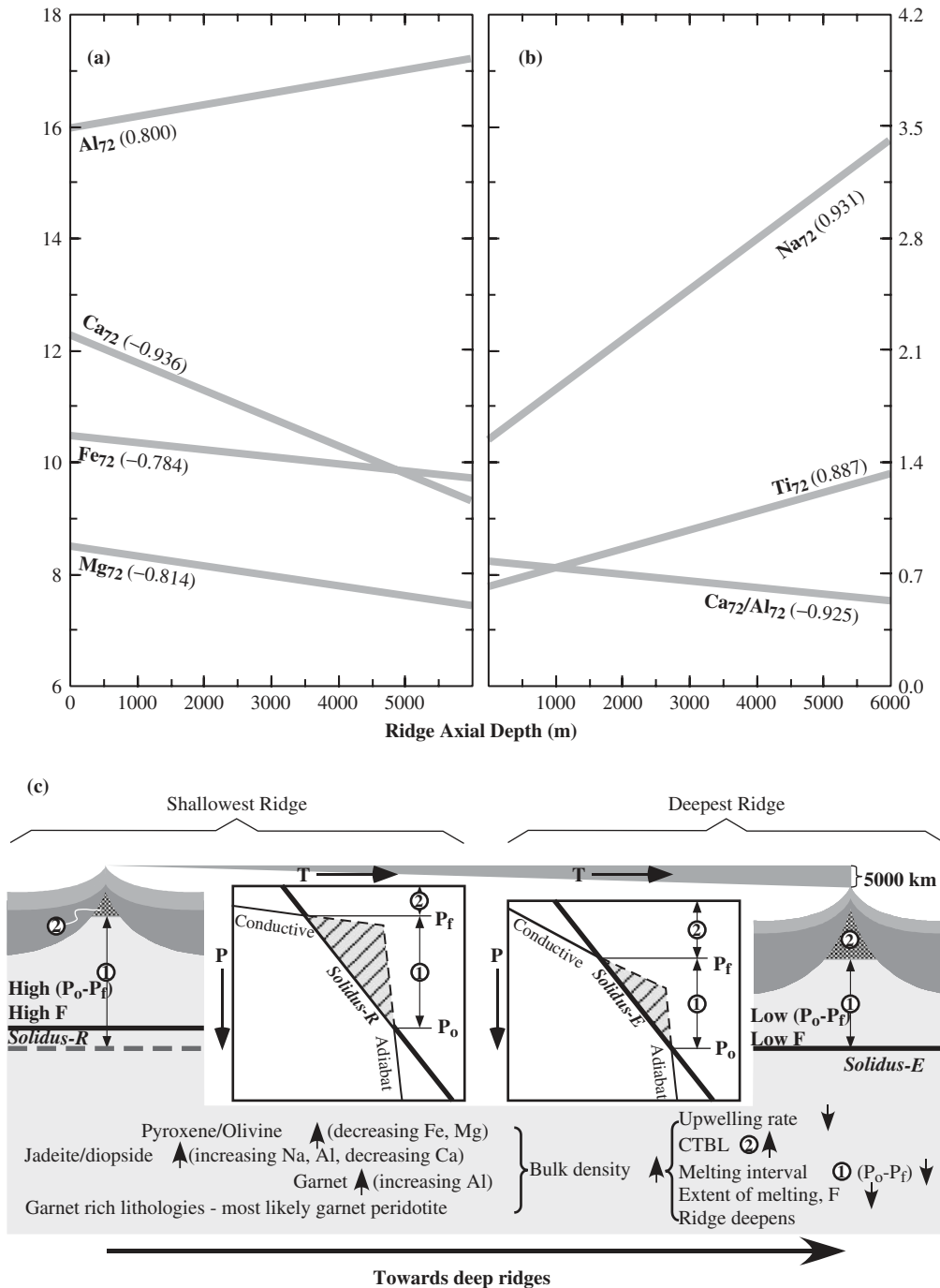
Fig. 15. (a) and (b) Variation of fractionation corrected (to $Mg^{\#} = 0{\cdot}72$) data trends from Fig. 9 vs ridge axial depth. (c) Schematic illustration of the concept of fertile mantle compositional controls on MORB composition and ridge depth variation on a global scale. The systematic compositional variation of MORB melts with ridge axial depth is partly inherited from fertile mantle compositional variation; that is, the fertile mantle becomes progressively more enriched (or less depleted) from beneath shallow ridges to beneath deep ridges, pointing to increasing modal garnet, jadeite/diopside ratio in clinopyroxene, and pyroxenes/olivine ratio, thus a progressively denser mineral assemblage towards beneath deep ridges. The stippled triangular regions in $P-T$ space illustrate conceptually the difference in melt production that is proportional to the height of decompression melting intervals ($P_o - P_f$; i.e. region '1'). The initial depth of melting (P_o) should be deeper for the more enriched (or less depleted) fertile mantle with solidus-E beneath deep ridges than for the more refractory fertile mantle with solidus-R beneath shallow ridges (thick solid lines) if $\Delta T_P \rightarrow 0$ beneath global ocean ridges. If the mantle beneath shallow ridges (e.g. the Reykjanes Ridge) is indeed hotter (e.g. $\Delta T_P \sim 40\,K$), then P_o would become slightly deeper (the thick dashed line), but P_o variation is likely to be small (see Electronic Appendix D for details). The final depth of melting (P_f) increases as the cold thermal boundary layer (CTBL; i.e. region '2') thickens with decreasing plate spreading rate (Niu & Hékinian, 1997a) and with increasing fertile mantle density as argued here. (See text for details.)
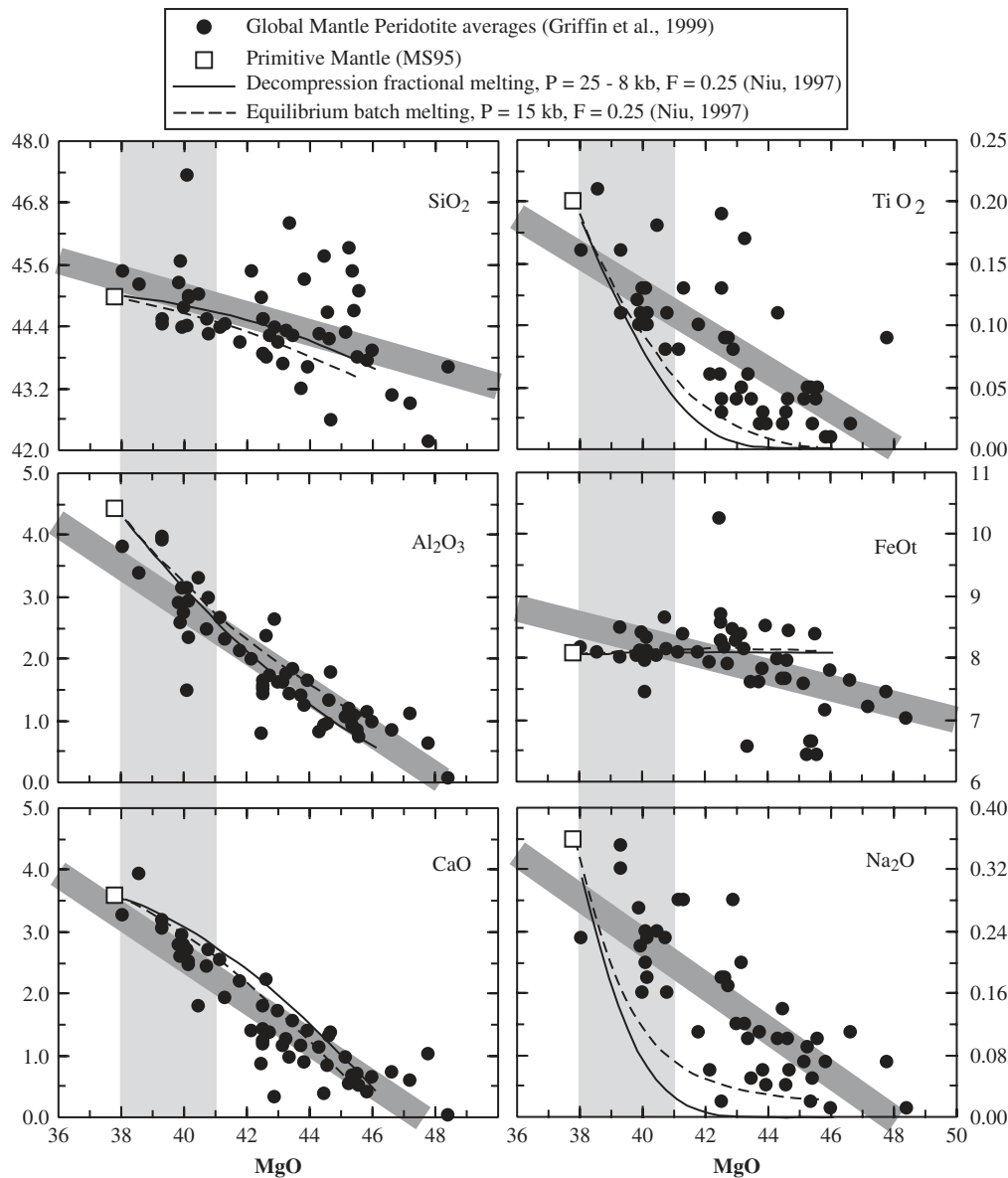
Fig. 16. MgO variation diagrams for 52 average bulk-rock compositions of mantle peridotites (xenoliths from various tectonic settings, orogenic massifs, abyssal peridotites and ophiolites, etc.) compiled by Griffin *et al.* (1999). For comparison, the primitive mantle (PM) composition of McDonough & Sun (1995) (MS95) and melting model residues of Niu (1997) using the PM are also plotted. The dark grey bands are exaggerated regression lines, which are used to estimate density variations with the extent of depletion (increasing MgO) in both spinel (Fig. 17) and garnet (Fig. 19) peridotite stability fields. The vertical grey bands between MgO = 38 and 41 wt% represent the likely fertile mantle source compositional range for MORB.

melting will make the residue compositionally more depleted and physically more buoyant, the overall density reduction is small in the spinel peridotite stability field (vs that in the garnet peridotite stability field; see below). As mantle melting residues beneath ocean ridges are located mostly in the spinel peridotite stability field, the density variation as a result of varying extents of melt extraction is small, and thus has limited

contribution to ridge axial depth variation (much less than considered in Figs 13 and 14).

Density of bulk-rock and constituent minerals as a function of melt depletion under garnet peridotite stability conditions

The density of garnet peridotites with the same bulk-rock compositions as those in Figs 16 and 17 should decline
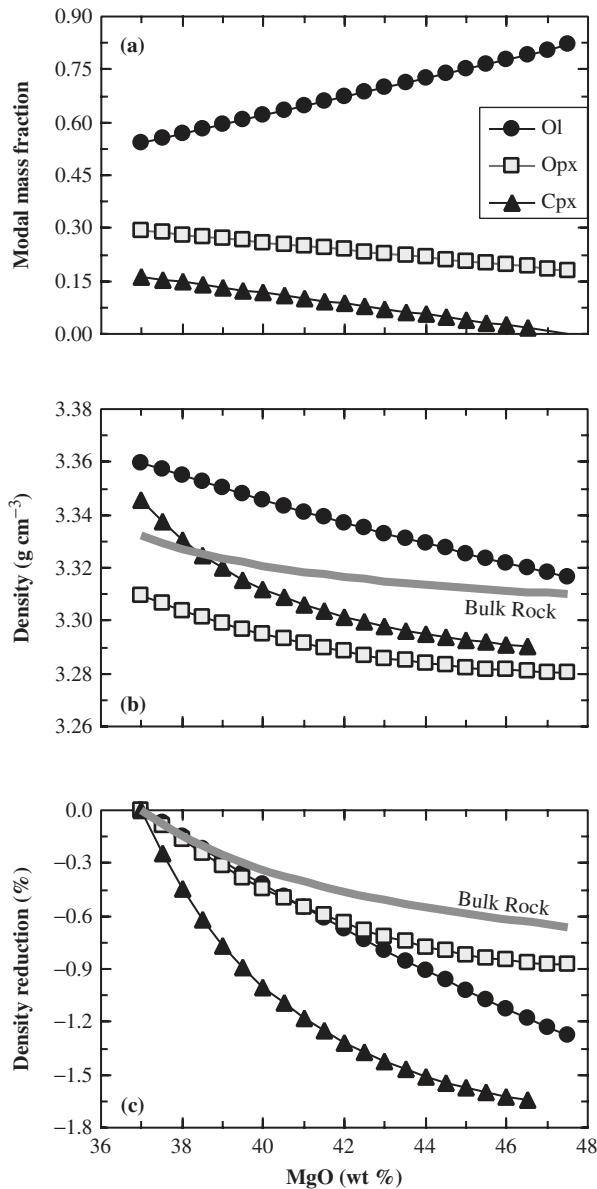
Fig. 17. (a) Modal variations (mass fraction) of olivine, opx and cpx calculated from bulk-rock compositions using the regression lines in Fig. 16 following Niu (1997). (b) Calculated mineral and bulk-rock density variation as a function of bulk-rock depletion (increasing wt% MgO resulting from melt extraction) using DENSCAL (Niu & Batiza, 1991b, 1991c) and the relationships of mineral compositions with bulk-rock MgO in abyssal peridotites (Niu *et al.*, 1997). The densities are calculated under the standard condition of 1 bar and 25°C (see text for details). (c) Density reduction of individual minerals and bulk-rock compositions as a result of depletion from an initial composition of MgO = 37%. It should be noted that bulk-rock density reduction as a result of depletion (from ∼37% to 47% MgO) is small, ∼0·6%, under spinel peridotite facies stability conditions, largely controlled by the Mg/Fe of the bulk-rock. Al_2O_3 in the bulk-rock is mostly locked in opx and cpx. Spinel mode is not calculated because of the practical difficulty, and because its composition changes (from high Al/Cr to low Al/Cr), but its abundance (∼0·5–1·0%) does not with progressive depletion. Thus, the small density contribution of spinel to the bulk-rock is essentially independent of bulk-rock depletion.
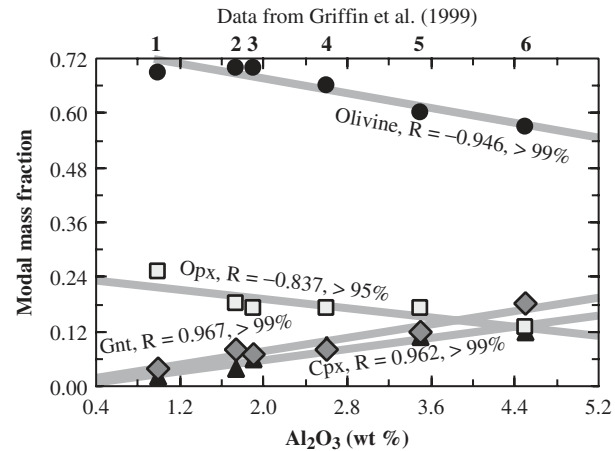
Fig. 18. Modal mineralogy of garnet peridotites as a function of bulk-rock Al_2O_3 (wt%) from Griffin *et al.* (1999, table 5). The sample suites are: 1, average of the Archons; 2, average of the Kaapvaal high-temperature suite; 3, average of the Protons; 4, average of the YETI suite; 5, average of the Tectons; 6, the Primitive Mantle composition of McDonough & Sun (1995). The large spread of Al_2O_3 contents covers the entire range of mantle garnet peridotites from primitive mantle to the most depleted harzburgites.

rapidly with increasing extent of depletion (increasing MgO) because Al_2O_3, and thus modal garnet, are depleted accordingly. The average bulk-rock compositions of garnet peridotites from representative xenolith suites allowed Griffin *et al.* (1999) to establish the modal systematics of garnet peridotite as a function of bulk-rock Al_2O_3 content. Figure 18 shows these modal systematics, which can be used to calculate mineral modes in garnet peridotites. The results are given in Fig. 19a. With increasing bulk-rock MgO (or melt depletion) (see Niu, 1997, fig. 8), both olivine and opx modes increase whereas garnet and cpx modes decrease, which is consistent with an incongruent melting relationship in the garnet peridotite stability field (O'Hara & Yoder, 1967; Herzberg, 1992): a Cpx + b Ol + c Gnt = 1·0 Melt + d Opx.

Figure 19b compares the density differences between garnet peridotite and spinel peridotite of the same bulk-composition (at a given MgO) and how the densities change with progressive depletion (increasing MgO). Figure 19c compares the density reduction (%) of spinel peridotite and garnet peridotite with progressive depletion (increasing MgO). The greater density of garnet peridotite than spinel peridotite of the same bulk-rock composition (Fig. 19b) is known to be determined by the dense garnet, and the greater density reduction of garnet peridotite than spinel peridotite with depletion again results from the decreasing garnet mode because of decreasing Al_2O_3 in the bulk-rock. This suggests that melting and melt extraction in the garnet (vs spinel) peridotite stability field can create spatially small-scale, but large-amplitude buoyancy variation in the mantle.
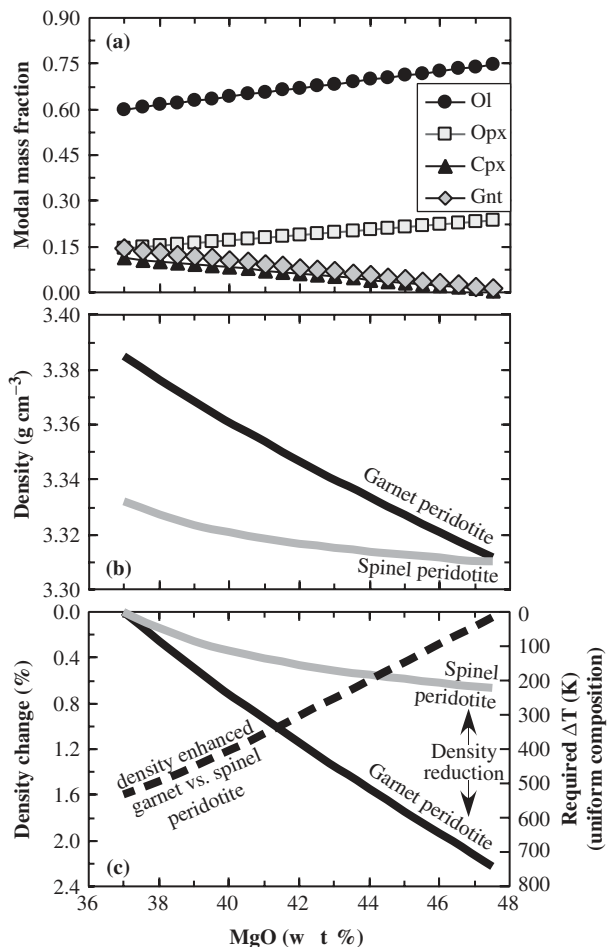
Fig. 19. (a) Modal variations of olivine, opx, cpx and garnet with the extent of depletion (increasing MgO) calculated using bulk-rock compositions (the regression lines in Fig. 16) and the relationships in Fig. 18. (b) Calculated bulk-rock densities of garnet peridotite and spinel peridotite (see Fig. 17) of the same bulk composition as a function of MgO wt%. The same density values (Fig. 17) as a function of MgO are assumed for olivine, opx and cpx, and a constant density of $3.6\,g/cm^3$ is assumed for garnet (small compositional variation makes little difference). The high density at low MgO and rapid reduction in density of the garnet peridotite with the extent of depletion (increasing MgO) results from garnet depletion because of bulk-rock Al_2O_3 depletion. (c) Density reduction (expressed as a percentage) of garnet peridotite (thick black line) and spinel peridotite (thick grey line) with increasing MgO content (i.e. depletion). The thick dashed line shows the per cent density increase from spinel peridotite to garnet peridotite for the same bulk composition. The right-hand side axis indicates the required temperature change (ΔT) to compensate density reduction due to compositional changes.

It should be noted that the density reduction of garnet peridotites from bulk-rock MgO = 37 to 42% can be as much as 1·2%, which is huge, and is equivalent to the effect of a temperature variation of ~400 K. Let us assume the fertile garnet peridotite is less depleted with 38% MgO in the deep ridge mantle and is more depleted with 41% MgO (possibly the most depleted fertile source) in the shallow ridge mantle. There would be 0·675% density difference (equivalent to an ~225 K temperature variation). This would require $D_C = 415$ km to account for $\Delta D_{RA} = 5$ km (see Fig. 14b and c). If we assume 40 wt% MgO in the shallow ridge mantle, there would be a 0·46% density difference (~153 K equivalent), which would require $D_C = 576$ km to account for $\Delta D_{RA} = 5$ km.

We emphasize the importance of garnet because the MORB source is largely in the garnet (vs spinel) peridotite stability field under subsolidus conditions, and because the compensation depth must be several hundreds of kilometers deep (see Figs 13 and 14) beneath ocean ridges where garnet is a stable phase. It is also conceptually important to note that density differences of 0·3–0·6% (equivalent to a temperature effect of 100–200 K) in the MORB mantle as a result of compositional variability (varying degrees of depletion; e.g. Fig. 16) is possible. This would require $D_C = 847$–458 km to account for the $\Delta D_{RA} = 5$ km. Because of the extremely slow rates of chemical diffusion, density differences caused by compositional differences can be 'permanent' (long-lived) and can persist in space and time in that depth range. However, it is physically unlikely to be able to maintain 100–200 K temperature difference in space and time beneath global ocean ridges to that depth range because of much faster thermal (vs chemical) diffusion, and effective thermal homogenization by large-scale lateral asthenospheric flow beneath the oceanic lithosphere (see above).

DISCUSSION
What controls the global ocean ridge axial depth variation?

We propose that plate tectonics dictates where ocean ridges begin and how they evolve, but that mantle density variation as a result of compositional (vs temperature) variation determines the axial depth of ridges. That is, mantle compositional variation results in mantle density variation that isostatically compensates the global ocean ridge axial relief of ~5 km. Figures 15, 18 and 19 show explicitly that less depleted mantle peridotites with higher Al_2O_3 content favor the formation of a greater amount of garnet, making the bulk-rock denser beneath deep ridges than beneath shallow ridges. We elaborate the argument further below.

The ridge axial depth varies from ~6000 m at the deep end of the spectrum (e.g. the Cayman Rise) to ~200 m at the shallow end (e.g. the Reykjanes Ridge) on a global scale. On local and regional scales, the ridge axial depth varies from <400 m along fast-spreading ridges (e.g. the East Pacific Rise, EPR) to as much as 1500 m within some segments of slow-spreading ridges (e.g. the Mid-Atlantic

Ridge, MAR). In general, ridge axial depth is a function of sub-ridge material density, which is in turn a function of temperature and mantle composition beneath the ridge. However, on local and regional scales, the ridge axial depth variation may also be caused by differential mantle upwelling rate or lithospheric flexure; that is, a component of 'dynamic topography' that is not in isostatic equilibrium. As our data averaging is done with respect to sample depths (i.e. 250 m depth intervals) regardless of geographical location (Fig. 5), the 'dynamic topography' effect has been averaged out. Thus, the global ridge axial depth variation (ΔD_{RA}) with its correlations with MORB chemistry (Tables 1 and 2; Figs 4, 5, 7, 9 and 10) is in isostatic equilibrium; that is, it reflects the effect of sub-ridge material density variation. We have demonstrated above that consideration of possible crustal thickness variation and residual mantle density variation, as well as ΔT_P cannot explain the $\Delta D_{RA} = 5$ km on a global scale. It follows that $\Delta D_{RA} = f(\Delta X_{MS})$ is largely true. One may argue that deep ridges such as the Cayman Rise, Southwest Indian Ridge and Arctic ridges are deep and spread slowly, so spreading rate may exert some control on ridge axial depth. This is not the case because (1) there is no apparent correlation between ridge axial depth and spreading rate on a global scale (Niu & Hekinian, 1997*a*; Rubin & Sinton, 2007), (2) shallow ridges such as the Reykjanes Ridge spread slowly (<25 mm/year), and (3) deep ridges such as the Australian Antarctic Discordance (AAD; >4 km) spread at an intermediate (~75 mm/year; not slow) rate.

Why is the AAD deep?

The AAD along the Southeast Indian Ridge (SEIR) is a unique feature of the global ocean ridge system that needs mention. The ADD is a complex ~400 km long segment of the SEIR with axial depth >4000 m, about 1000–1500 m deeper than the adjacent 'normal ridges'. The AAD has been interpreted as a cold ridge segment (e.g. Forsyth *et al.*, 1987; Ritzwoller *et al.*, 2003) or even the site of downwelling where the Pacific and Indian asthenospheres meet because of ancient cold subducted oceanic lithosphere (crust + lithospheric mantle) that is sinking beneath the AAD (Gurnis *et al.*, 1998). Whether the mantle beneath the AAD is cold or not is unknown, but we do know that the AAD is deep, and must be underlain by dense material. If the mantle is cold and the 'cold anomaly' is currently maintained in the uppermost <150 km of the mantle (Ritzwoller *et al.*, 2003), then the 'anomaly' beneath the AAD would have to be unrealistically cold (theoretically >900 K colder). If, on the other hand, the 'cold anomaly' extends down to the 660 km discontinuity (Gurnis *et al.*, 1998), then the mean temperature beneath the AAD would be ~150 K colder than that beneath the Reykjanes Ridge (in the context of our model in Figs 13 and 14). Otherwise, a fertile mantle compositional anomaly would

better explain the deep topographic anomaly. As the subducted lithosphere has finite dimension, and because the AAD is a local or regional anomaly, the cold-slab model with an ~150 K thermal anomaly extending down to the 660 km discontinuity (vs <150 km) is physically plausible.

Because 'the SEIR is the only ridge to override an old subduction zone', and 'this overriding is probably the reason why the AAD is a unique feature of the global system of ridges' (Gurnis *et al.*, 1998, p. 1503), the cold-slab model for the AAD, if correct, does not apply to deep ridges elsewhere because of the much longer wavelengths (thousands of kilometers) of ridge axial depth variation than the ~400 km of the AAD.

Why is Iceland shallow?

Iceland is another unique feature of the global mid-ocean ridge system with its voluminous melt production and anomalous ridge axial depth above sea level. These features have resulted in the classification of Iceland as a 'hotspot'. This 'hotspot' has been widely accepted as the surface manifestation of a hot and deeply rooted thermal mantle plume originating from great depths—perhaps from the core–mantle boundary or from the base of the upper mantle. The 'enriched' incompatible element and radiogenic isotope characteristics of Iceland rocks have led to the wide acceptance that mantle plumes are derived from enriched fertile mantle peridotite sources at depths significantly deeper than the more depleted MORB mantle source. However, the enrichment or fertility of the plume source with its high Fe/Mg (and high Al_2O_3) makes the plume source 'negatively' buoyant relative to MORB mantle, creating physical difficulties for the rise of the Iceland plume (O'Hara, 1973). An excess mantle potential temperature of >300 K relative to the ambient MORB mantle may explain the Iceland hotspot by (1) possible thermal buoyancy, (2) buoyant crust and (3) buoyant residual mantle as a result of a large extent of melting caused by the hot mantle source. However, Foulger *et al.* (2005) have contested the mantle plume model for Iceland, suggesting that it is inconsistent with a thermal mantle plume because (1) there is no evidence for a hot mantle source (probably less than a few tens of degrees Kelvin hotter than the MORB mantle), and (2) it is a shallow feature, certainly confined to the upper mantle. These researchers offered an alternative to explain the melting anomaly by invoking the presence of abundant eclogite (or mantle peridotite fertilized by 'resorbed eclogite') in the Iceland mantle source left behind by the subducted oceanic crust of the Caledonian suture. They suggested that such a source can produce several times more melt than normal mantle peridotite without the need for high temperatures.

The plate separation rate at Iceland is slow, ~25 mm/year (full rate). Therefore, it is not possible to explain the large melt volumes of Iceland by a low extent

of melting of a large amount of source material per unit time, as the residual mantle cannot be carried away fast enough [even recognizing the along-axis flow (Niu & Hékinian, 2004)]. Hence, a large extent of melting for a given parcel of fertile mantle is necessary. The presence of abundant eclogite with a lower solidus temperature than the 'host' peridotite would certainly help. However, there is a physical problem with this model. The density of the bulk-rock fertile peridotite mantle (assumed to be $3·35\,g/cm^3$ for simplicity) will be increased by addition of the dense eclogite component (assumed to be $3·50\,g/cm^3$). The fertile mantle density will increase (%) by $\sim0·05 \times$ eclogite (vol.%). That is, 3% eclogite addition increases the bulk-rock density by $\sim0·15\%$ (equivalent to decreasing the temperature by $\sim45\,K$), and 6% eclogite addition increases the bulk-rock density by $\sim0·3\%$ (equivalent to decreasing the temperature by $\sim90\,K$). If 10% eclogite is needed to produce more melt to make the thick ($>20\,km$) Iceland crust (vs $\sim6\,km$ 'normal ocean crust'), then the Iceland fertile mantle would be $\sim0·5\%$ denser (or $\sim150\,K$ cooler) than the MORB source mantle. The implication of such a simple calculation is that to add the dense eclogitic material into the Iceland fertile mantle would make Iceland the deepest, not the shallowest ridge (see the discussion on the AAD above). If the mantle potential temperature beneath Iceland is the same as that of the normal ocean ridge mantle, then Iceland must be underlain by compositionally depleted (low Fe/Mg, Al_2O_3) and physically buoyant mantle material (like subcontinental lithospheric material?).

If the Reykjanes Ridge is indeed affected by the Iceland 'plume', then we can infer from Fig. 15 that it is physically plausible that the Iceland fertile mantle is more depleted in terms of major elements (also see possible depletion in K_2O from Fig. 5). We thus have the Iceland paradox. Our model for the Reykjanes Ridge can help with the Iceland scenario, but cannot explain the overall Iceland phenomena. Perhaps the Iceland fertile mantle is rich in volatiles (i.e. wet melting of a depleted peridotite source), or maybe it is indeed hot (i.e. hot melting of depleted peridotite source). We do not have an answer to the Iceland paradox, but we propose the need for a more serious, comprehensive and unbiased examination of the Iceland problem.

What controls the global MORB compositional variation?

The systematic and correlated variations of MORB chemistry with ridge axial depth (Figs 4, 5, 7 and 9) suggest that they are both consequences of a common cause in the mantle. We maintain that this is the major element compositional variation in the mantle beneath global ocean ridges. The observed MORB compositional variation (Figs 9 and 15), after fractionation correction

to $Mg^{\#} = 0·72$, results from the combination of two different, but genetically related, processes: (1) mantle source inheritance; (2) melting process enhancement.

The systematic variations of Al_{72}, Na_{72}, Ti_{72}, K_{72}, Ca_{72}, Ca_{72}/Al_{72}, Fe_{72} and Mg_{72} in MORB melts with increasing ridge axial depth (Figs 5b, 9 and 15) are consistent with a progressively more enriched (or less depleted) peridotite source from beneath shallow ridges to beneath deep ridges. Figure 15c shows schematically that fertile mantle compositional (mineralogical and lithological) variation leads to progressively denser fertile mantle from beneath shallow ridges to beneath deep ridges. In response to plate separation, the denser mantle rises slowly, resulting in a reduced melting rate, deepened conductive geotherm, shortened melting column, and thus lowered extents of melting from beneath shallow ridges to beneath deep ridges. That is, deep ridge MORB melts have the signatures of lower extents of melting than shallow ridge MORB melts (Figs 5b, 9 and 15). For example, among all the major and minor elements, the small decrease of Fe_{72} and Mg_{72} from shallow ridges to deep ridges is also consistent with decreasing extent of melting (Fig. 1).

It may sound counterintuitive that the less depleted (or enriched) fertile mantle beneath deep ridges melts less than the more depleted and refractory mantle beneath shallow ridges. However, the explanation is straightforward if we consider the two fundamental factors that control melting: (1) adiabatic upwelling; (2) enthalpy of melting. Without adiabatic upwelling, there would be no decompression melting, and no melt would be produced regardless of how fertile the peridotite source was. The retarded upwelling rate beneath deep ridges (greater density) leads to retarded melt production by decompression, and hence a lower melting rate than beneath shallow ridges. Furthermore, the restricted amplitude of upwelling (greater density) beneath deep ridges results in a short decompression melting interval $(P_o - P_f)$ (Fig. 15). Thus shallower ridges are characterized by overall higher extents of melting relative to the mantle beneath deeper ridges, producing more melt per unit time. The observation that the most depleted abyssal peridotites still have cpx as a residual phase (Dick & Natland, 1996; Niu & Hékinian, 1997a, 1997b) indicates that ocean ridge melting does not eliminate cpx. That is, partial melting from a few per cent to high extents before cpx elimination, which mostly occurs in the olivine–opx–cpx–spinel four-phase field, does not require excess heat as long as adiabatic upwelling occurs. This reasoning is corroborated by an experimental study of 'second-stage melting' (Duncan & Green, 1987), and by the refractory MORB melts from the Garret Transform formed as a result of intra-transform extension-induced decompression melting of previous melting residues beneath the EPR axis (Hékinian et al., 1995; Niu & Hékinian, 1997b; Wendt et al., 1999).

What controls the initial depth (P_o) of melting?

It is conceptually correct that a hotter parcel of mantle that rises adiabatically will intersect the solidus and begin to melt deeper than a cooler parcel of mantle. On the other hand, as the solidus is a material property, its location in P–T space is composition dependent. As we argue that the fertile MORB source is less refractory beneath deep ridges than beneath shallow ridges, and if T_P is similar beneath all ridges (i.e. $\Delta T_P \leq 50$ K), then the initial depth of melting would be slightly shallower (not deeper) beneath shallow ridges as indicated in Fig. 15c. If T_P beneath shallow ridges (e.g. the Reykjanes Ridge) were indeed ~40 K hotter than T_P beneath deep ridges, this would place the onset of melting at a slightly deeper level indicated by the thick dashed line on the left of Fig. 15c. The existing data indicate that the onset of melting increases (1) by ~0·89 kbar per 10 K T_P increase (McKenzie & Bickle, 1988; Langmuir *et al.*, 1992), (2) by ~0·29 kbar per 1·0 unit $Mg^\#$ decrease (e.g. from 91 to 90) in the peridotite source, and (3) by 0·76 kbar per 0·05 wt% total alkali ($Na_2O + K_2O$) increase (Herzberg *et al.*, 2000; Hirschmann, 2000; Niu *et al.*, 2001). By assuming that the shallow ridge mantle is ~40 K hotter, and more depleted (2 $Mg^\#$ units higher, 0·05 wt% total alkalis less) than the deep ridge mantle, then the ascending mantle beneath the shallow ridge would intersect the solidus ~2 kbar (+ 3·5 − 0·76 − 0·58 = 2·16 kbar) deeper than the mantle beneath the deep ridge, which is well within the uncertainties. This suggests that the net effect of source composition and small T_P contributions on the initial depth of melting is likely to be very small, and the depth of initial melting beneath the global ocean ridge system must be very similar. The extent of melting, which is proportional to $P_o − P_f$, is thus largely controlled by the final depth of melting (Niu & Hékinian, 1997*a*).

What controls the final depth (P_f) of melting?

Klein & Langmuir (1987) and McKenzie & Bickle (1988) assumed that decompression melting continues up to the Moho beneath ocean ridges. Niu & Batiza (1991*a*), however, showed that mantle melting beneath ocean ridges stops at levels significantly deeper than the Moho because MORB chemistry is inconsistent with melting to the Moho and with basic magma crystallization immediately above the Moho. Shen & Forsyth (1995) emphasized the importance of conductive cooling in determining the final depth of melting, but did not specify what could cause varying depth of melting cessation. Detailed studies of abyssal peridotites and MORB chemistry suggest that the final depth of melting (P_f) increases with decreasing spreading rate (Niu, 1997, 2004; Niu & Hékinian, 1997*a*, 1997*b*; Niu *et al.*, 1997). All these results, together with the

S-wave seismic velocity data of Zhang & Tanimoto (1993), are consistent with melting cessation at depths >30 km beneath very slow-spreading ridges, but significantly less than 30 km beneath fast-spreading ridges (Niu, 1997; Niu & Hékinian, 1997a). The argument of spreading-rate control on the depth of melting cessation is based on the concept that ridges are mostly passive features and the rate of adiabatic upwelling beneath ocean ridges is proportional to the rate of plate separation. This concept applies here.

The final depth of melting (P_f) is the result of a balance between conductive cooling to the seafloor and adiabatic upwelling of hot mantle (Fig. 15c). As the temperature on the seafloor is fixed, ~0–3°C, the boundary condition for the conductive cooling is fixed. Hence, P_f is controlled by the rate of asthenospheric upwelling, which is known to depend on spreading rate (e.g. Reid & Jackson, 1981; Niu, 1997; Niu & Hékinian, 1997a) and also on mantle density variation as we argue here. The fertile mantle with greater density beneath deep ridges retards the rate and restricts the amplitude of the upwelling, and allows conductive cooling to penetrate to a great depth, forcing melting to stop at a deeper level than beneath shallow ridges (Fig. 15c).

Why are MORB melts more evolved at shallow ridges?

Figures 4, 6 and 7 show that MORB melts erupted at shallower ridges are progressively more evolved with $Mg^\#$ decreasing from ~0·68 at deep ridges to 0·55 at shallow ridges. The explanation is straightforward. As discussed above, the rate of decompression melting, the extent of melting and the overall melt production increase from beneath deep ridges to beneath shallow ridges. It follows that there is progressively more frequent melt supply to the crust from beneath deep ridges to beneath shallow ridges. As a result, a progressively longer-lived magma chamber is better developed beneath shallower ridges. The key is that the crust at shallower ridges will have a higher time-averaged mean temperature (warmer) than the crust at deeper ridges. Such a crustal-level thermal state allows melts supplied to shallower ridges to experience more advanced extents of differentiation or evolution (resulting in low $Mg^\#$). In contrast, infrequent melt supply at deep ridges leads to crustal cooling, and the melts would experience limited extents of differentiation before freezing (high $Mg^\#$), or may even freeze in the mantle before reaching the crust. The latter case [i.e. the lack of erupted lavas at some deep (e.g. the Arctic) and slow-spreading (e.g. the 15°N MAR) ridges] has led to the view of 'amagmatic' spreading in the recent literature (see Dick *et al.*, 2003; Michael *et al.*, 2003).

The above argument that the extent of MORB melt differentiation is a result of mantle melt production and melt supply frequency is consistent with similar arguments on MORB petrogenesis as a function of spreading rate

(Sinton & Detrick, 1992; Niu & Hékinian, 1997a, 1997b; Rubin & Sinton, 2007).

Why do we invoke garnet-rich peridotites rather than eclogites or garnet pyroxenites beneath deep ridges?

Our inferred chemical and mineralogical compositions of the fertile MORB mantle beneath deep ridges are qualitatively consistent with the presence of progressively more abundant recycled eclogites or garnet pyroxenites, which have been argued to be important in the source regions of oceanic basalts (e.g. Hirschmann & Stolper, 1996; Pertermann & Hirschmann, 2003). However, the lack of pyroxenites (converted from eclogites and garnet pyroxenites) in mantle melting residues (abyssal peridotites) sampled from the seafloor (e.g. Dick & Fisher, 1984; Dick et al., 1984; Dick, 1989; Niu & Hékinian, 1997b) suggests that eclogites and garnet pyroxenites may not be abundant in MORB source regions (also see Niu et al., 2002; Niu & O'Hara, 2003). It is possible that pyroxenites may be melted out, which explains the absence of such lithologies in abyssal peridotites. However, pyroxenites are not observed in mantle samples collected from Arctic ridges, where the extent of melting diminishes (Michael et al., 2003). All these observations suggest that although eclogites and garnet pyroxenites must exist in the mantle, as inferred from massif peridotites and mantle xenoliths, they must be volumetrically insignificant (vs garnet-rich peridotites) to explain the observed global correlations of ridge axial depth and MORB chemistry. Recycled eclogites (+ lithospheric mantle) may indeed exist beneath the AAD (see above), but the AAD is a unique feature of the global system of ocean ridges.

Why is there a stronger garnet signature in MORB melts from deep ridges than from shallow ridges?

MORB major element compositions and melting relationships recorded in abyssal peridotites (Niu, 1997) are consistent with MORB being generated largely in the spinel peridotite stability field, but incipient melts formed in the garnet peridotite stability field are expected because of volatile-induced melting at greater depths. High Sm/Yb ratios in some MORB melts are interpreted as indicating the presence of garnet as a residual phase in the source region. ^{230}Th excesses in MORB melts are also interpreted as reflecting the presence of garnet in the melting region (Beattie, 1993). This interpretation is further supported by Hf isotope systematics (Salters & Hart, 1989). Salters (1996) reported an interesting observation based on Hf–Nd isotopes that MORB melts from deep ridges (e.g. Cayman Rise and AAD) have stronger garnet signatures than MORB melts from shallow ridges (e.g. Kolbeinsey Ridge and Reykjanes Ridge). To be consistent with Fe$_8$-based interpretations, Salters (1996) proposed that the onset of melting below shallow ridges starts

deeper (high Fe$_8$) than for deep ridges (low Fe$_8$), and that shallow ridges are characterized by a columnar-shaped melting region with a narrow base in the garnet stability field, whereas melts from deep ridges sample a triangular-shaped melting regime with a wide base where garnet is a stable phase. Although this interpretation is interesting, it is not necessary to invoke peculiarly different geometries of the melting regions beneath shallow and deep ridges. A straightforward interpretation is that the intensity of the garnet signature in MORB melts is inversely related to the extent of dilution; it is diluted less in melts produced by low extents of melting beneath deep ridges and is diluted more in melts produced by high extents of melting beneath shallow ridges (Niu et al., 1999).

Are ocean ridges of shallow or deep origin?

Recognizing that ocean ridges are mostly passive features in response to plate separation, we accept that ocean ridges are of shallow origin. The ridge process-affected part of the mantle may be limited to the upper 150–200 km of the asthenosphere (e.g. Ekström & Dziewonski, 1998) although the actual affected depth may vary, depending on the viscosity structure with depth and plate separation rate. The plate separation rate is important because it is proportional to the ridge suction force that drives the material flow towards ridges to form the crust and much of the lithospheric mantle (Niu & Hékinian, 2004). If mantle viscosity increases exponentially with depth, then the material needs at the ridge must be supplied by lateral asthenospheric (low-velocity zone) flow towards ridges. This leads to the inevitable decoupling of the ridgeward asthenospheric flow and the superjacent plate movement away from the ridge (Niu et al., 1999; Niu & Hékinian, 2004). The roughly 150–200 km depth that may be affected by passive ridge melting processes is perhaps the very limit that Klein & Langmuir (1987) placed on the $D_C = 150$–200 km, although this depth range is inconsistent with a $\Delta T_P = 250$ K as proposed in their model.

We have demonstrated above that mantle potential temperature variation, if significant at all (probably $\Delta T_P \leq 50$ K) (plus the density contributions of varying crustal thickness and residual mantle; see Figs 13 and 14), is inadequate to explain the global ridge axial relief of $\Delta D_{RA} = 5$ km, and fertile mantle compositional variation is required. The latter is predicted to be characterized by progressively more enriched (or less depleted) fertile peridotite with higher Al_2O_3 (and co-variations of other major element oxides seen in Fig. 16) and thus more dense peridotite from beneath shallow ridges to beneath deep ridges. This explains not only the ridge axial depth variation, but also its correlations with MORB chemistry on a global scale (Figs 4, 5, 7, 9 and 10).

Using the peridotite data compiled by Griffin et al. (1999) (Fig. 16) as a reference, it is clear that the density

reduction (Fig. 19) from less depleted peridotite (say MgO = 38 wt%) to the most depleted (yet still fertile) peridotite must be in the range of 0·3–0·6%, with 0·6% being the maximum required to produce the observed MORB compositional variation. This requires a compensation depth of 847 km for 0·3% density variation and 458 km for 0·6% density reduction without considering the effects of phase transitions (i.e. the 410 km and 660 km discontinuities). Consideration of the effects of phase transitions shallows the compensation depth, but the latter remains likely to be within the 410–660 km transition zone, if not in the lower mantle. It follows that whereas ocean ridges form or originate as a consequence of plate tectonics, and are thus mostly passive features, the actual controls on the surface expression of ridges (first-order ridge axial depth variation on a global scale), rate of mantle upwelling, extent of melting, melt production, and melt composition are likely to be deep.

Therefore, ocean ridges are of shallow origin, but their working is largely controlled by deep processes as well as the effect of plate spreading rate variation at shallow levels. An intriguing question is if such small compositional variations (large enough to cause significant density differences; see both Fig. 15 and Fig. 19) have any effect on the behavior of the 410 km (if not the 660 km) discontinuity. If so, is seismology sensitive enough to detect this behavior along the global ocean ridge system as a function of ridge axial depth variation, recognizing the fact that the ridge axial depth variation correlates with MORB chemistry? We consider this to be a worthwhile topic for future study towards a better understanding of how the Earth works.

SUMMARY

(1) The petrological parameters Na_8 and Fe_8 of Klein & Langmuir (1987) have been widely used as indicators of the extents and pressures of mantle melting beneath ocean ridges, and have also been used to elucidate the petrogenesis of basalts from other tectonic settings. However, these parameters are unreliable.

(2) Fe_8 is the essence of the Klein & Langmuir (1987) and Langmuir *et al.* (1992) theory, and is used to compute the mantle solidus depth (P_o) and temperature (T_o). It is the values and range of Fe_8 that allowed Klein & Langmuir (1987) to argue that mantle temperature variation of up to 250 K is required to explain the global ocean ridge systematics. This interpreted 250 K range actually applies to normal ocean ridges unaffected by 'hotspots'. We found no convincing evidence that calculated values for P_o, T_o, ΔT_o, ΔP_o and ΔT_P on the basis of Fe_8 have any significance.

(3) MORB melts, when corrected for fractionation effects to a constant $Mg^\# = 0·72$, reflect mostly signals of mantle processes because melts with $Mg^\# = 0·72$ are in equilibrium with mantle olivine of $Fo_{89·6}$ (vs evolved olivine of $Fo_{88·1–79·6}$ in equilibrium with melts of Fe_8). The Fe_{72} values of the global depth-interval averages range from 7·5 to 8·5, which, using the model of Klein & Langmuir (1987) and Langmuir *et al.* (1992), would give $\Delta T_P = 41$ K (vs ~250 K based on Fe_8) beneath global ocean ridges unaffected by 'hotspots'. The lack of Fe_{72}–Si_{72} and Si_{72}–ridge depth correlations provides no evidence that MORB melts preserve pressure signatures as a function of ridge axial depth. There is thus no convincing evidence for $\Delta T_P > 50$ K beneath global ocean ridges unaffected by 'hotspots'.

(4) The significance of ridge axial depth correlations with MORB chemistry is better revealed by averaging out possible effects of other processes such as spreading rate variation, local-scale mantle source heterogeneity, melting region geometry variation, and dynamic topography on regional and segment scales using actual sample depths regardless of geographical locations within each of the 22 ridge depth intervals of 250 m on a global scale.

(5) Significant correlations exist between ridge axial depth and fractionation-uncorrected raw data for major and minor element oxides except for SiO_2, MnO and P_2O_5. The systematic variations of TiO_2, Al_2O_3, CaO, Na_2O, K_2O and CaO/Al_2O_3 with ridge axial depth are largely inherited from the parental magmas. The systematic FeO increase, MgO decrease and the associated $Mg^\#$ decrease towards shallow ridges are consistent with progressively advanced degrees of melt differentiation towards shallow ridges. High extents of melting and frequent melt supply from mantle to the crust at shallow ridges favor development of a warm crust and long-lived magma chambers (as in the case of the fast-spreading EPR), resulting in advanced degrees of differentiation (low $Mg^\#$), whereas low extents of melting and infrequent melt supply from mantle to the crust at deep ridges lead to a cold crust and prohibit the development of long-lived magma chambers, such that the melt may freeze in the mantle or experience limited degrees of differentiation before solidification in the crust.

(6) Significant correlations between ridge axial depth and fractionation-corrected MORB chemistry (Ti_{72}, Al_{72}, Fe_{72}, Mg_{72}, Ca_{72}, Na_{72}, K_{72} and Ca_{72}/Al_{72}) exist. The fractionation correction has recovered the expected positive FeO–MgO correlations in model primary melts and melts produced in peridotite melting experiments. The MORB compositional systematics at $Mg^\# = 0·72$ result from the combination of two different, but genetically related

processes—mantle source inheritance and melting process enhancement.

(7) The correlations between MORB chemistry and ridge axial depth suggest that they are both consequences of a common mantle process. The subsolidus mantle major element compositional (mineralogical, lithological, etc.) variation, not mantle temperature variation, results in mantle density variation that isostatically compensates the global ridge axial relief of $\Delta D_{RA} = 5$ km as well as correlations with MORB chemistry. That is, a progressively more enriched (or less depleted) fertile source (i.e. high Al_2O_3 and Na_2O, and low CaO/Al_2O_3) beneath deep ridges ensures a greater amount of modal garnet (high Al_2O_3) and high jadeite/diopside ratios in clinopyroxene (high Na_2O and Al_2O_3, and lower CaO), making a denser mantle, and thus deeper ridges. The small decrease in Fe_{72} and Mg_{72} in MORB melts with increasing ridge axial depth is consistent with the more enriched (or less depleted) source with lower modal olivine beneath deep ridges. Hence, MORB chemistry is a manifestation of subsolidus mantle composition.

(8) The extent of mantle melting is controlled by the initial (P_o) and final (P_f) depths of melting, i.e. $P_o - P_f$. P_o is expected to increase with increasing T_P and mantle fertility. The lack of convincing evidence for huge T_P variation and the small effect of MORB mantle compositional variation on P_o suggest limited P_o variation beneath global ocean ridges. Hence, the extent of melting depends largely on P_f, which is controlled by the rate of asthenospheric upwelling, and increases with decreasing plate separation rate. We emphasize here that the rate and amplitude of the mantle upwelling also depend on mantle density variation. The fertile mantle with greater density beneath deep ridges retards the rate and restricts the amplitude of the upwelling, leads to reduced melting rate by decompression, gives ways to conductive cooling to a great depth, forces melting to stop at a great depth with a short melting interval $(P_o - P_f)$, and thus produces less melt, and probably thinner magmatic crust in comparison with the less dense fertile mantle beneath shallow ridges.

(9) The variability of fertile mantle composition is limited by whether the source rock is fertile enough to produce melts with expected compositions by reasonable extents of melting. If the fertile mantle beneath deep ridges, for example, has $MgO = 38$ wt%, then the density reduction for the more refractory peridotites must be in the range of 0·3–0·6% to produce the observed MORB compositional variation. It would require compensation depths of 847 km for 0·3% density variation and 458 km for 0·6% density variation. Therefore, whereas ocean ridges are of shallow origin,

their working is largely controlled by deep processes as well as the effect of plate spreading rate variation at shallow levels. With phase changes considered, the compensation depths would be within the 410–660 km transition zone (if not deeper). Do such small compositional variations have observable effects on the behavior of the 410 km and 660 km seismic discontinuities?

(10) The anomalously deep AAD may be the prime candidate for a cold sub-ridge mantle. Elsewhere, it is subsolidus mantle compositional (vs temperature) variation that determines the mineralogy, lithology and density variations that control the 5 km global ocean ridge relief and its correlation with the first-order MORB compositional variation. Current mantle plume debate on Iceland exposes an 'Iceland Paradox', which awaits a resolution.

ACKNOWLEDGEMENTS

SUPPLEMENTARY DATA

Supplementary data for this paper are available at *Journal of Petrology* online.

REFERENCES

Albarède, F. (1992). How deep do common basaltic magmas form and differentiate? *Journal of Geophysical Research* **97**, 10997–11009.

Baker, M. B. & Stolper, E. M. (1994). Determining the composition of high-pressure mantle melts using diamond aggregates. *Geochimica et Cosmochimica Acta* **58**, 2811–2827.

Batiza, R. & Niu, Y. (1992). Petrology and magma chamber processes at the East Pacific Rise ∼9°30'N. *Journal of Geophysical Research* **97**, 6779–6797.

Beattie, P. (1993). Uranium-thorium disequilibria and partitioning on melting of garnet peridotite. *Nature* **363**, 63–65.

Brodholt, J. P. & Batiza, R. (1989). Global systematics of unaveraged mid-ocean ridge basalt compositions: Comments on 'Global correlations of ocean ridge basalt chemistry with axial depth and crustal thickness by Klein, E. M. and Langmuir, C. H.'. *Journal of Geophysical Research* **94**, 4231–4239.

Bryan, W. B. & Dick, H. J. B. (1982). Contrasted abyssal basalt liquidus trends: evidence for mantle major element heterogeneity. *Earth and Planetary Science Letters* **58**, 15–26.

Cannat, M. (1996). How thick is the magmatic crust at slow-spreading oceanic ridges? *Journal of Geophysical Research* **101**, 2847–2857.

Castillo, P. R., Natland, J. H., Niu, Y. & Lonsdale, P. (1998). Sr, Nd, and Pb isotopic variation along the Pacific ridges from 53 to 56°S: Implications for mantle and crustal dynamic processes. *Earth and Planetary Science Letters* **154**, 109–125.

Castillo, P. R., Klein, E., Bender, J., Langmuir, C., Shirey, S., Batiza, R. & White, W. (2000). Petrology and Sr, Nd, and Pb isotope geochemistry of mid-ocean ridge basalts from 11°45'N to 15°N segments of the East Pacific Rise. *Geochemistry, Geophysics, Geosystems* **1**, paper number 1999GC000024.

Christensen, N. I. (1972). Abundance of serpentinites in oceanic crust. *Journal of Geology* **80**, 709–719.

Detrick, R., Collins, J., Stenphen, R. & Swift, S. (1994). *In situ* evidence for the nature of the seismic layer 2/3 boundary in oceanic crust. *Nature* **370**, 288–290.

Dick, H. J. B. (1989). Abyssal peridotites, very slow spreading ridges and ocean ridge magmatism. In: Saunders, A. D. & Norry, M. J. (eds) *Magmatism in the Ocean Basins. Geological Society, London, Special Publications* **42**, 71–105.

Dick, H. J. B., Fisher, R. L. & Bryan, W. B. (1984a). Mineralogical variability of the uppermost mantle along mid-ocean ridges. *Earth and Planetary Science Letters* **69**, 88–106.

Dick, H. J. B. & Fisher, R. L. (1984b). Mineralogic studies of the residues of mantle melting: Abyssal and alpine-type peridotites. In: Kornprobst, J. (ed.) *The Mantle and Crustal–Mantle Relationships—Mineralogical, Petrological, and Geodynamic Processes of the Third International Kimberlite Conference*, Vol. 2, Amsterdam : Elsevier, pp. 295–308.

Dick, H. J. B. & Natland, J. H. (1996). Late-stage melt evolution and transport in the shallow mantle beneath The East Pacific Rise. In: Mével, C., Gills, K. M. & Allan, J. F. (eds) *Proceedings of the Ocean Drilling Program, Scientific Results, 147*. College Station, TX: College Station, pp. 103–134.

Dick, H. J. B., Lin, J. & Schouten, H. (2003). An ultraslow-spreading class of ocean ridge. *Nature* **426**, 405–412.

Duncan, R. A. & Green, D. H. (1987). The genesis of refractory melts in the formation of oceanic crust. *Contributions to Mineralogy and Petrology* **96**, 326–342.

Ekström, G. & Dziewonski, A. M. (1998). The unique anisotropy of the Pacific upper mantle. *Nature* **394**, 168–172.

Falloon, T. J. & Green, D. H. (1987). Anhydrous partial melting of MORB pyrolite and other peridotite compositions at 10 k bar: Implications for the origin of MORB glasses. *Mineralogy and Petrology* **37**, 181–219.

Falloon, T. J. & Green, D. H. (1988). Anhydrous partial melting of peridotite from 8 to 35 kb and the petrogenesis of MORB. *Journal of Petrology, Special Lithosphere Issue*, 379–414.

Falloon, T. J., Green, D. H., Hatton, C. J. & Harris, K. L. (1988). Anhydrous partial melting of a fertile and depleted peridotite from 2 to 30 kb and application to basalt petrogenesis. *Journal of Petrology* **29**, 1257–1282.

Fang, N. & Niu, Y. (2003). Late Paleozoic ultramafic lavas in Yunnan, Southwest China and their geodynamic significance. *Journal of Petrology* **44**, 141–158.

Forsyth, D. W. (1992). Geophysical constraints on mantle flow and melt generation beneath mid-ocean ridges. In: Phipps Morgan, J., Blackman, D. K. & Sinton, J. M. (eds) *Mantle Flow and Melt Generation at Mid-ocean Ridges. American Geophysical Union Monograph* **71**, 1–66.

Forsyth, D. W., Ehrenbard, R. L. & Chapin, S. (1987). Anomalous upper mantle beneath the Australian–Antarctic Discordance. *Earth and Planetary Science Letters* **84**, 471–478.

Foulger, G. R., Natland, J. H. & Anderson, D. L. (2005). Genesis of the Iceland melt anomaly by plate tectonic processes. In: Foulger, G. R., Natland, J. H., Presnall, D. C. & Anderson, D. L. (eds) *Plates, Plumes, and Paradigms. Geological Society of America, Special Papers* **388**, 595–625.

Green, D. H. (1971). Compositions of basaltic magmas as indicators of conditions origin: Application to oceanic volcanism. *Philosophical Transaction of the Royal Society of London* **A268**, 707–725.

Green, D. H. (1973). Experimental studies on a modal upper mantle composition at high pressure under water-saturated and water-undersaturated conditions. *Earth and Planetary Science Letters* **19**, 37–53.

Green, D. H. & Falloon, T. J. (1998). Pyrolite: A Ringwood concept and its current expression. In: Jackson, I. (ed.) *The Earth's Mantle, Composition, Structure, and Evolution*. Cambridge: Cambridge University Press, pp. 311–380.

Green, D. H. & Falloon, T. J. (2005). Primary magmas at mid-ocean ridges, 'hotspots,' and other intraplate settings: Constraints on mantle potential temperature. In: Foulger, G. R., Natland, J. H., Presnall, D. C. & Anderson, D. L. (eds) *Plates, Plumes, and Paradigms. Geological Society of America, Special Papers* **388**, 217–248.

Green, D. H. & Ringwood, A. E. (1963). Mineral assemblages in a model mantle composition. *Journal of Geophysical Research* **68**, 937–945.

Green, D. H. & Ringwood, A. E. (1964). Fractionation of basalts at high pressures. *Nature* **201**, 1276–1279.

Green, D. H. & Ringwood, A. E. (1967). The genesis of basaltic magmas. *Contributions to Mineralogy and Petrology* **15**, 103–190.

Green, D. H. & Ringwood, A. E. (1970). Mineralogy or peridotite compositions under upper mantle conditions. *Physics of the Earth and Planetary Interiors* **3**, 359–371.

Green, D. H., Hibberson, W. O. & Jaques, A. L. (1979). Petrogenesis of mid-ocean ridge basalts. In: McElhinny, M. W. (ed.) *The Earth: Its Origin, Structure and Evolution*. London: Academic Press, pp. 265–290.

Green, D. H., Falloon, T. J., Eggins, S. M. & Yaxley, G. M. (2001). Primary magmas and mantle temperatures. *European Journal of Mineralogy* **13**, 437–451.

Griffin, W. L., O'Reilley, S. Y. and Ryan, C. G. (1999). The composition and origin of subcontinental lithosphere. In: Fei, Y, Bertka, C. M. & Mysen, B. O. (eds) Mantle Petrology: Field Observations and High-Pressure Experimentation: A Tribute to Francis R. (Joe) Boyd. *Geochemical Society Special Publication* **6**, 13–46.

Gurnis, M., Muller, R. D. & Moresi, L. (1998). Cretaceous vertical motion of Australia and the Australian–Antarctic Discordance. *Science* **279**, 1499–1504.

Hékinian, R., Bideau, D., Herbért, R. & Y. Niu., (1995). Magmatic processes at upper mantle–crustal boundary zone: Garrett transform (EPR South). *Journal of Geophysical Research* **100**, 10163–10185.

Herzberg, C. (1992). Depth and degree of melting of komatiites. *Journal of Geophysical Research* **97**, 4521–4540.

Herzberg, C. & O'Hara, M. J. (1998). Phase equilibrium constraints on the origin of basalts, picrites, and komatiites. *Earth-Science Reviews* **44**, 39–79.

Herzberg, C. & O'Hara, M. J. (2002). Plume-associated ultramafic magmas of Phanerozoic age. *Journal of Petrology* **43**, 1857–1883.

Herzberg, C., Raterron, P. & Zhang, J. (2000). New experimental observations on the anhydrous solidus for peridotite KLN-1. *Geochemistry, Geophysics, Geosystems* **1**, paper number 2000GC00089.

Herzberg, C., Asimow, P. D., Arndt, N., Niu, Y., Albarède, F., Lesher, C. M., Fitton, J. G., Cheadle, M. J. & Saunders, A. D. (2007). Temperatures in ambient mantle and plumes: Constraints from basalts, picrites and komatiites. *Geochemistry, Geophysics, Geosystems* (in press).

Hess, H. H. (1962). History of the ocean basins. In: *Petrologic Studies: A Volume to Honour A.F. Buddington.* Denver, CO: Geological Society of America, pp. 599–620.

Hirose, K. & Kushiro, I. (1993). Partial melting of dry peridotites at high pressures: Determination of compositions of melts segregated from peridotite using aggregates of diamonds. *Earth and Planetary Science Letters* **114**, 477–489.

Hirschmann, M. M. (2000). Mantle solidus: Experimental constraints and the effects of peridotite composition. *Geochemistry, Geophysics, Geosystems* **1**, paper number 2000GC000070.

Hirschmann, M. M. & Stolper, E. M. (1996). A possible role for garnet pyroxenite in the origin of the 'garnet signature' in MORB. *Contributions to Mineralogy and Petrology* **124**, 185–208.

Jaques, A. L. & Green, D. H. (1980). Anhydrous melting of peridotite at 0–15 kb pressure and the genesis of tholeiitic basalts. *Contributions to Mineralogy and Petrology* **73**, 287–310.

Kinzler, R. J. (1997). Melting of mantle peridotite at pressures approaching the spinel to garnet transition: Application to mid-ocean ridge basalt petrogenesis. *Journal of Geophysical Research* **102**, 853–874.

Kinzler, R. J. & Grove, T. L. (1992). Primary magmas of mid-ocean ridge basalts, 2, applications. *Journal of Geophysical Research* **97**, 6907–6926.

Klein, E. M. & Langmuir, C. H. (1987). Global correlations of ocean ridge basalt chemistry with axial depth and crustal thickness. *Journal of Geophysical Research* **92**, 8089–8115.

Klein, E. M. & Langmuir, C. H. (1989). Local versus global variation in ocean ridge basaltic composition: A reply. *Journal of Geophysical Research* **94**, 4241–4252.

Kushiro, I. (1996). Partial melting of a fertile mantle peridotite at high pressures: An experimental study using aggregates of diamond. *Geophysical Monograph, American Geophysical Union* **95**, 109–122.

Langmuir, C. H. (1989). Geochemical consequences of *in situ* crystallization. *Nature* **340**, 199–205.

Langmuir, C. H., Klein, E. M. & Plank, T. (1992). Petrological systematics of mid-ocean ridge basalts: Constraints on melt generation beneath ocean ridges. In: Phipps Morgan, J., Blackman, D. K. & Sinton, J. M. (eds) *Mantle Flow and Melt Generation at Mid-ocean Ridges. American Geophysical Union Monograph* **71**, 183–280.

Lecroart, P., Albarède, F. & Cazenave, A. (1997). Correlations of mid-ocean ridge basalt chemistry with the geoid. *Earth and Planetary Science Letters* **153**, 37–55.

McDonough, W. F., Sun, & S.-s. (1995). The composition of the Earth. *Chemical Geology* **120**, 223–253.

McKenzie, D. & Bickle, M. J. (1988). The volume and composition of melt generated by extension of the lithosphere. *Journal of Petrology* **29**, 625–679.

Michael, P. J, Langmuir, C. H., Dick, H. J. B., Snow, J. E., Goldstein, S. L., Graham, D. W., Lehnert, K., Kurras, G., Jokat, W., Muhe, R. & Edmonds, H. N. (2003). Magmatic and amagmatic seafloor generation at the ultraslow-spreading Gakkel ridge, Arctic Ocean. *Nature* **423**, 956–961.

Natland, J. H. (1989). Partial melting of a lithologically heterogeneous mantle: Inferences from crystallisation histories of magnesian abyssal tholeiites from the Siqueiros Fracture Zone. In: Saunders, A. D. & Norry, M. J. (eds) *Magmatism in the Ocean Basins. Geological Society, London, Special Publications* **42**, 41–70.

Niu, Y. (1997). Mantle melting and melt extraction processes beneath ocean ridges: Evidence from abyssal peridotites. *Journal of Petrology* **38**, 1047–1074.

Niu, Y. (2004). Bulk-rock major and trace element compositions of abyssal peridotites: Implications for mantle melting, melt extraction and post-melting processes beneath ocean ridges. *Journal of Petrology* **45**, 2423–2458.

Niu, Y. (2005). Generation and evolution of basaltic magmas: Some basic concepts and a hypothesis for the origin of the Mesozoic–Cenozoic volcanism in eastern China. *Geological Journal of China Universities* **11**, 9–46.

Niu, Y. & Batiza, R. (1991a). An empirical method for calculating melt compositions produced beneath mid-ocean ridges: application for axis and off-axis (seamounts) melting. *Journal of Geophysical Research* **96**, 21753–21777.

Niu, Y. & Batiza, R. (1991b). *In-situ* densities of silicate melts and minerals as a function of temperature, pressure, and composition. *Journal of Geology* **99**, 767–775.

Niu, Y. & Batiza, R. (1991c). DENSCAL: A program for calculating the densities of silicate melts and minerals as a function of temperature, pressure, and composition in magma generation environment. *Computers and Geosciences* **17**, 679–687.

Niu, Y. & Batiza, R. (1993). Chemical variation trends at fast and slow spreading ridges. *Journal of Geophysical Research* **98**, 7887–7902.

Niu, Y. & Batiza, R. (1994). Magmatic processes at the Mid-Atlantic Ridge ~26° S. *Journal of Geophysical Research* **99**, 19719–19740.

Niu, Y. & Batiza, R. (1997). Trace element evidence from seamounts for recycled oceanic crust in the eastern Pacific mantle. *Earth and Planetary Science Letters* **148**, 471–483.

Niu, Y. & Hékinian, R. (1997a). Spreading rate dependence of the extent of mantle melting beneath ocean ridges. *Nature* **385**, 326–329.

Niu, Y. & Hékinian, R. (1997b). Basaltic liquids and harzburgitic residues in the Garrett transform: A case study at fast-spreading ridges. *Earth and Planetary Science Letters* **146**, 243–258.

Niu, Y. & Hékinian, R. (2004). Ridge suction drives plume–ridge interactions. In: Hékinian, R., Stoffers, P. & Cheminée, J.-L. (eds) *Oceanic Hotspots.* New York: Springer, pp. 285–307.

Niu, Y. & O'Hara, M. J. (2003). The origin of ocean island basalts (OIB): A new perspective from petrology, geochemistry and mineral physics considerations. *Journal of Geophysical Research* **108**, doi:10.1029/2002JB002048.

Niu, Y., Waggoner, D. G., Sinton, J. M. & Mahoney, J. J. (1996). Mantle source heterogeneity and melting processes beneath

seafloor spreading centers: The East Pacific Rise, 18°–19°S. *Journal of Geophysical Research* **101**, 27711–27733.

Niu, Y., Langmuir, C. H. & Kinzler, R. J. (1997). The origin of abyssal peridotites: A new perspective. *Earth and Planetary Science Letters* **152**, 251–265.

Niu, Y., Collerson, K. D., Batiza, R., Wendt, J. I. & Regelous, M. (1999). The origin of E-Type MORB at ridges far from mantle plumes: The East Pacific Rise at 11°20'N. *Journal of Geophysical Research* **104**, 7067–7087.

Niu, Y., Bideau, D., Hékinian, R. & Batiza, R. (2001). Mantle compositional control on the extent of melting, crust production, gravity anomaly and ridge morphology: a case study at the Mid-Atlantic Ridge 33–35°N. *Earth and Planetary Science Letters* **186**, 383–399.

Niu, Y., Regelous, M. Wendt, J. I., Batiza, R. & O'Hara, M. J. (2002). Geochemistry of near-EPR seamounts: Importance of source vs process and the origin of enriched mantle component. *Earth and Planetary Science Letters* **199**, 329–348.

Niu, Y., O'Hara, M. J. & Pearce, J. A. (2003). Initiation of subduction zones as a consequence of lateral compositional buoyancy contrast within the lithosphere: A petrologic perspective. *Journal of Petrology* **44**, 851–866.

O'Hara, M. J. (1965). Primary magmas and the origin of basalts. *Scottish Journal of Geology* **1**, 19–40.

O'Hara, M. J. (1967). Crystal–liquid equilibria and the origins of ultramafic nodules in igneous rocks. In: Wyllie, P. J. (ed.) *Ultramafic and Related Rocks*. New York: John Wiley, pp. 346–349.

O'Hara, M. J. (1968a). Are ocean floor basalts primary magmas? *Nature* **220**, 683–686.

O'Hara, M. J. (1968b). The bearing of phase equilibria studies in synthetic and natural systems on the observation of volcanic products. *Physics of the Earth and Planetary Interiors* **3**, 236–245.

O'Hara, M. J. (1970). Upper mantle composition inferred from laboratory experiments and observation of volcanic products. *Physics of the Earth and Planetary Interiors* **3**, 236–245.

O'Hara, M. J. (1973). Non-primary magmas and dubious mantle plume beneath Iceland. *Nature* **243**, 507–508.

O'Hara, M. J. (1977). Geochemical evolution during fractional crystallization of a periodically refilled magma chamber. *Nature* **266**, 503–507.

O'Hara, M. J. (1985). Importance of the 'shape' of the melting regime during partial melting of the mantle. *Nature* **314**, 58–62.

O'Hara, M. J. (1995). Trace element geochemical effects of integrated melt extraction and 'shaped' melting regime. *Journal of Petrology* **36**, 1111–1132.

O'Hara, M. J. & Herzberg, C. (2002). Interpretation of trace element and isotope features of basalts: Relevance of field relations, petrology, major element data, phase equilibria, and magma chamber modeling in basalt petrogenesis. *Geochimica et Cosmochimica Acta* **66**, 2167–2191.

O'Hara, M. J. & Mathews, R. E. (1981). Geochemical evolution in an advancing, periodically replenished, periodically tapped, continuously fractionating magma chamber. *Journal of the Geological Society, London* **138**, 237–277.

O'Hara, M. J. & Yoder, H. S. (1963). Partial melting of the mantle. *Carnegie Institution of Washington Yearbook* **62**, 66–71.

O'Hara, M. J. & Yoder, H. S. (1967). Formation and fractionation of basic magmas at high pressures. *Scottish Journal of Geology* **3**, 67–117.

O'Reilly, S. Y. & Griffin, W. L. (1988). Mantle metasomatism beneath western Victoria, Australia: I, Metasomatic processes in Cr-diopside lherzolites. *Geochimica et Cosmochimica Acta* **52**, 433–447.

Pertermann, M. & Hirschmann, M. M. (2003). Partial melting experiments on a MORB-like pyroxenite between 2 and 3 GPa: Constraints on the presence of pyroxenite in basalt source regions from solidus location and melting rate. *Journal of Geophysical Research* **108**, doi:10.1029/2000JB000118.

Phipps Morgan, J., Morgan, W. J., Zhang, Y.-S. & Smith, W. H. F. (1995). Observational hints for a plume-fed, suboceanic asthenosphere and its role in mantle convection. *Journal of Geophysical Research* **100**, 12753–12767.

Presnall, D. C. & Gudfinnsson, G. H. (2007). Origin of the Oceanic Lithosphere. *Journal of Petrology* **49**, 613–630.

Presnall, D. C., Dixon, J. R., O'Donnell, T. H. & Dixon, S. A. (1979). Generation of mid-ocean ridge tholeiites. *Journal of Petrology* **20**, 3–35.

Presnall, D. C., Gudfinnsson, G. H. & Walter, M. J. (2002). Generation of mid-ocean ridge basalts at pressures from 1 to 7 GPa. *Geochimica et Cosmochimica Acta* **66**, 2073–2090.

Regelous, M., Niu, Y., Wendt, J. I., Batiza, R., Greig, A. & Collerson, K. D. (1999). An 800 ka record of the geochemistry of magmatism on the East Pacific Rise at 10°30'N: Insights into magma chamber processes beneath a fast-spreading ocean ridge. *Earth and Planetary Science Letters* **168**, 45–63.

Reid, I. & Jackson, H. R. (1981). Oceanic spreading rate and crustal thickness. *Marine Geophysical Research* **5**, 165–172.

Ritzwoller, M. H., Shapiro, N. M. & Leahy, G. M. (2003). The Australian–Antarctic mantle anomaly as the principal cause of the Australian–Antarctic Discordance. *Journal of Geophysical Research* **108**, doi:10.1029/2003JB002522.

Roeder, P. L. & Emslie, R. F. (1970). Olivine–liquid equilibrium. *Contributions to Mineralogy and Petrology* **29**, 275–289.

Rubin, K. H. & Sinton, J. M. (2007). Inferences on mid-ocean ridge thermal and magmatic structure from MORB compositions. *Earth and Planetary Science Letters* **260**, 257–276.

Salters, V. J. M. (1996). The generation of mid-ocean ridge basalts from the Hf and Nd isotope perspective. *Earth and Planetary Science Letters* **141**, 109–123.

Salters, V. J. M. & Hart, S. R. (1989). The hafnium paradox and the role of garnet in the source of mid-ocean ridge basalts. *Nature* **342**, 420–422.

Shen, Y. & Forsyth, D. W. (1995). Geochemical constraints on initial and final depth of melting beneath mid-ocean ridges. *Journal of Geophysical Research* **100**, 2211–2237.

Sinton, J. M. & Detrick, R. S. (1992). Mid-ocean ridge magma chambers. *Journal of Geophysical Research* **97**, 197–216.

Stolper, E. A. (1980). phase diagram for mid-ocean ridge basalts: Preliminary results and implications for petrogenesis. *Contributions to Mineralogy and Petrology* **74**, 13–27.

Sun, S.-s. & McDonough, W. F. (1989). Chemical and isotopic systematics in ocean basalt: Implication for mantle composition and processes. In: Saunders, A. D. & Norry, M. J. (eds) *Magmatism in the Ocean Basins. Geological Society, London, Special Publications* **42**, 313–345.

Turcotte, D. L. & Phipps Morgan, J. (1992). Magma migration and mantle flow beneath a mid-ocean ridge. In: Phipps Morgan, J., Blackman, D. K. & Sinton, J. M. (eds) *Mantle Flows and Melt Generation at Mid-ocean Ridges. American Geophysical Union Monograph* **71**, 155–182.

Walker, D., Shibata, T. & DeLong, S. E. (1979). Abyssal tholeiites from the Oceanographer Fracture Zone, II, Phase equilibria and mixing. *Contributions to Mineralogy and Petrology* **70**, 111–125.

Wendt, J. I., Regelous, M., Niu, Y., Hékinian, R. & Collerson, K. D. (1999). Geochemistry of lavas from the Garrett Transform

Fault: insights into mantle heterogeneity beneath the eastern Pacific. *Earth and Planetary Science Letters* **173**, 271–284.

White, R. S., McKenzie, D. P. & O'Nions, R. K. (1992). Oceanic crustal thickness from seismic measurements and rare earth elements inversions. *Journal of Geophysical Research* **97**, 19683–19715.

White, R. S., Minshull, T. A., Bickle, M. J. & Robinson, C. J. (2001). Melt generation at very slow-spreading oceanic ridges: Constraints from geochemical and geophysical data. *Journal of Petrology* **42**, 1171–1196.

Wyllie, P. J. (1973). Experimental petrology and global tectonics: a preview. In: Wyllie, P. J. (ed.) *Experimental Petrology and Global Tectonics. Tectonophysics* **17**, 189–209.

Zhang, Y.-S. & Tanimoto, T. (1993). High resolution global upper mantle structure and plate tectonics. *Journal of Geophysical Research* **98**, 9793–9823.